Thesis for The Degree of Licentiate of Engineering

Alternative materials for proton exchange membranes

Synthesis of imidazole containing solid and liquid electrolytes

Eva Dahlqvist

Department of Chemistry and Chemical Engineering
Chalmers University of Technology
Gothenburg, Sweden, 2026

Alternative materials for proton exchange membranes
Synthesis of imidazole containing solid and liquid electrolytes

Eva Dahlqvist

ISSN 2026:08

Department of Chemistry and Chemical Engineering
Division of Applied Chemistry
Chalmers University of Technology
SE-412 96 Göteborg,
Sweden
Phone: +46(0)31 772 1000

Printed by Chalmers Digitaltryck,
Gothenburg, Sweden 2026.

Alternative materials for proton exchange membranes

Synthesis of imidazole containing solid and liquid electrolytes

Eva Dahlqvist

Department of Chemistry and Chemical Engineering
Chalmers University of Technology

Abstract

To achieve a sustainable future with significantly reduced greenhouse gas emissions, hydrogen has been proposed as an alternative energy carrier. With promising applications in balancing the electricity grid and in the transport sector, proton exchange membrane fuel cells (PEMFCs) are a key technology for realizing such a hydrogen-based society. While already commercially available, current PEMFCs are limited to operating temperatures of about 80 °C due to constraints imposed by the commonly used membrane materials. This restriction reduces the overall efficiency of both the cell and the fuel cell system. Consequently, there is a strong interest in alternative materials that exhibit high proton conductivity at elevated temperatures while maintaining mechanical and chemical stability under acidic conditions. Imidazole, a highly stable amphoteric molecule, offers both hydrogen-bonding capability and proton-accepting sites, making it a promising candidate for such applications. This thesis investigates the synthesis and fundamental properties of materials incorporating imidazole into their structures. Specifically, imidazole is introduced into a covalent organic framework by linker-exchange, into functionalized bases for the synthesis of Brønsted acidic protic ionic liquids, and into aqueous solutions. The developed method for synthesizing an imidazole-linked covalent organic framework provides an alternative route that yields increased crystallinity and porosity. The functionalization of alkylated imidazole with electron-withdrawing groups increased the acidity of the resulting protic ionic liquid, but decreased its ionic conductivity. Furthermore, investigating imidazole in aqueous solution provided insight into its supramolecular organization and its influence on the proton dissociation of sulfonic acid groups. A deeper understanding of imidazole and its effective incorporation into materials contributes to the knowledge required for the rational design of next-generation proton-conducting systems.

Keywords

Covalent Organic Frameworks, Imidazole, Proton Conduction, Protic Ionic Liquids, Proton Exchange Membranes, Synthesis.

List of Publications

This thesis is based on the following publications:

[**I**] **Eva Dahlqvist***, Eduardo M. Morais*, Anna Martinelli, *Synthesis and characterization of new imidazolium based protic ionic liquids obtained by nitro- and cyano-functionalization*
Journal of Molecular Liquids 415 (Dec 2024), 126269.
*Equal contribution

[**II**] Nicole Abdou, **Eva Dahlqvist**, Anna Martinelli, *Local interactions and dynamics in aqueous imidazole probed by vibrational and NMR spectroscopy*
Submitted.

[**III**] **Eva Dahlqvist**, Gregor J. Lauter, Danbo Wang, Nina Kann, Karl Börjesson, Ganna Gryn'ova, Yizhou Yang, Anna Martinelli, *Imidazole-linked covalent organic frameworks through post-synthetic linker-exchange*
Manuscript.

My Contributions

Paper I: Partook in the synthesis and characterization of the ionic liquids studied in the publication, as well as the interpretation of the experimental data. I co-wrote the article and took part in the editing process, in particular during the revision process.

Paper II: Conceptualized the idea of this specific liquid mixture, collected vibrational spectra, analyzed the experimental results, and co-drafted all sections together with co-authors.

Paper III: Designed the study and conceptualized the idea. Performed the synthesis and parameter screening for the conditions. Collected and interpreted all experimental data. Wrote and edited the article with input from coauthors.

Acknowledgment

First and foremost, I would like to extend my sincere gratitude to my incredible supervisory team, Nina, Yizhou, Karl, and Anna, for your guidance, support, and thoughtful input throughout this work. I would also like to thank my COF co-conspirators, Danbo and Gregor. Thank you both for always being up for discussing new ideas, embarking on new projects, and stepping in with a helping hand whenever my research needed it.

To all my colleagues, thank you for making this such an inspiring, supportive, and wonderful place to work. It has made all the difference.

To my family and friends, for your never-ending support and for providing me with all the joy a person could wish for. Especially when my research is not going to plan, with chemistry doing what it does best (i.e., not what I wanted it to do), your chats, laughs, and care are what make my day.

Thank you all for making this journey not only possible, but genuinely enjoyable.

This work has been supported by the Competence Center TechForH2, which is hosted by Chalmers University of Technology and is financially supported by the Swedish Energy Agency (P2021-90268) and the member companies Volvo, Scania, Siemens Energy, GKN Aerospace, PowerCell, Oxeon, RISE, Stena Rederier AB, Johnsson Matthey, and Insplorion.

Abbreviations

2-MTHF	2-Methyltetrahydrofuran
AEMFC	Anion exchange membrane fuel cell
AIL	Aprotic ionic liquid
AMFC	Alkaline fuel cell
ASE	Atomic Simulation Environment
ATR	Attenuated total reflectance
CCM	Catalyst-coated membrane
COF	Covalent organic framework
DCC	Dynamic covalent chemistry
DMF	Dimethylformamide
DMFC	Direct methanol fuel cell
DOSY NMR	Diffusion-ordered spectroscopy nuclear magnetic resonance
DRIFT	Diffuse reflectance infrared fourier transform
DSC	Differential scanning calorimetry
FTIR	Fourier transform infrared spectroscopy
GDL	Gas diffusion layers
HOR	Hydrogen oxidation reaction
IL	Ionic liquid
ILD	Interlayer distance
ILS	Interlayer slipping
IR	Infrared
LT-PEMFC	Low-temperature proton exchange membrane fuel cells
MEA	Membrane electrode assembly
MOF	Metal–organic frameworks
NMP	N-Methyl-2-pyrrolidone
NMR	Nuclear magnetic resonance
ORR	Oxygen reduction reaction
PA	Phosphoric acid
PAFC	Phosphoric acid fuel cell
PBI	Polybenzimidazole
PEM	Proton exchange membrane
PEMFC	Proton exchange membrane fuel cell
PFAS	Per- and polyfluoroalkyl substances
PFSA	Perfluorosulfonic acid

PIL	Protic ionic liquid
POP	Porous organic polymer
PPF	Porous polymer framework
PTFE	Polytetrafluoroethylene
PXRD	Powder X-ray diffraction
RCSR	Reticular chemistry structure resource
SCXRD	Single-crystal X-ray diffraction
SOFC	Solid oxide fuel cell
TCAT	4-tert-butylcatechol
TGA	Thermogravimetric Analysis
THF	Tetrahydrofuran
UFF	Universal force field
USAXS	Ultrasmall-angle X-ray scattering

Contents

Part I

Summary

Chapter 1

Introduction

The proton is one of the most influential particles in all of chemistry. Despite its simplicity and small size, this single positively charged nucleus governs a range of processes, including acid-base chemistry, energy flow in both biology and modern energy technologies, and the influence on molecular intramolecular and intermolecular structures through tautomerization and hydrogen bonding. Unlike many other charge carriers, the proton rarely travels alone and instead moves through networks, hopping between molecules or relaying through hydrogen bonds in a dynamic manner. This ability to access these pathways makes proton transport uniquely efficient and fundamentally different from the motion of larger ions. What is especially fascinating about the proton is how strongly its behavior depends on its chemical environment. In water, it forms transient species and moves rapidly via relay mechanisms, while in structured materials, its motion can be guided, restricted, or enhanced by molecular design. This provides an opportunity to control proton transport by tailoring material properties, enabling access to the behavior required for applications such as catalysis, sensing, and energy technologies.

A chemical structure that favorably interacts with protons is the imidazole ring, and it is these two, proton and imidazole, that will take center stage throughout this thesis. The imidazole structure, while large in comparison to the proton, is a deceptively simple yet multifaceted molecule.[1] This heterogeneous five-membered ring is polar, planar, and aromatic, contains two distinct nitrogen atoms, and has two equivalent tautomeric forms, as the hydrogen atom can be located on either nitrogen atom (Figure 1.1). These nitrogens are, however, of different character: one donates its lone pair to the aromatic sextet, while the other is more pyridine-like, with a non-delocalized lone pair that imparts basic properties. Together, these features give imidazole its amphoteric nature, allowing it to act as both an acid and a base, accepting protons at the N^3 position and donating from N^1. While it is a white solid on its own, it is commonly found in larger molecules and polymers, with applications in medicine, ionic liquids, and polybenzimidazoles. Imidazole is easily protonated to form imidazolium salts or to participate in proton conduction and can be alkylated to form ionic liquids. Imidazole also plays an important role in the

human body. It is part of histidine, which is responsible for activating many enzymes, and is present in other bioactive substances, for example, exhibiting antibacterial,[2,3] anti-inflammatory,[4] anti-fungal,[5] and anti-tumor[6] properties.

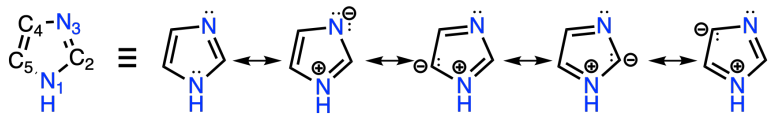

Figure 1.1: The structure of imidazole and its resonance forms.

The versatility of imidazole, both in its chemical behavior and range of applications, makes it a compelling building block in the design of functional materials. With increasing focus on the development of materials capable of efficient proton conduction under diverse conditions, imidazole offers promising opportunities in both solid and liquid systems, supporting multiple modes of proton transport. Proton conduction is particularly significant in the context of hydrogen-based energy technologies, where proton exchange membrane (PEM) fuel cells are widely regarded as a key technology for enabling a future hydrogen-based economy. The membrane through which proton conduction occurs is an electrolyte, usually comprised of a solid and a liquid component.

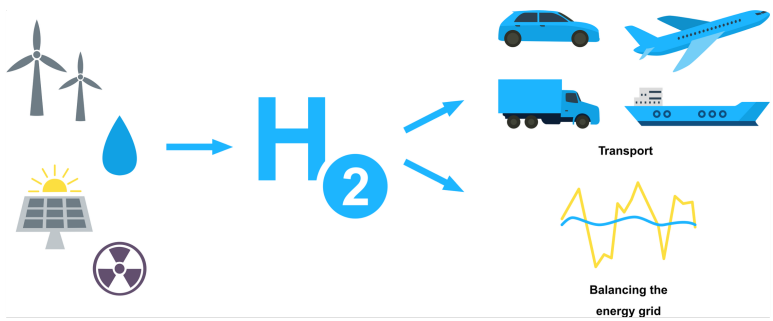

Figure 1.2: An environmentally sustainable future might include establishing a hydrogen-based system, in which energy sources with low emissions can be used to produce hydrogen. Hydrogen can then be used for different purposes, such as balancing the energy grid as well as transportation.

1.1 Scope and aim of thesis

This thesis explores the incorporation of imidazole into various materials and furthers the understanding of its behavior in solution. More precisely, imidazole is incorporated into the solid porous architecture of covalent organic frameworks via an alternative synthesis route to achieve high crystallinity, as well as into the cation of functionalized protic ionic liquids, investigating how the use of electron-withdrawing groups may affect the acidic strength and properties of the resulting compound.

While this thesis will place these materials in the context of alternative materials for inclusion in PEMFCs, no practical attempts to do so will be made; rather, these studies are intended to further our fundamental understanding of these materials and their synthesis methods, thereby enabling better design of these systems and expanding access to materials in the future.

Imidazole is a small yet versatile and multifaceted molecule. This five-membered aromatic heterocycle is polar, planar, and amphoteric, owing to its two distinct nitrogen atoms, one contributing basic character and the other participating in the aromatic system. As a result, imidazole can act as both a hydrogen-bond donor and acceptor, enabling rich and dynamic intermolecular interactions. These properties make imidazole particularly attractive for applications in proton-conducting systems, such as proton exchange membrane fuel cells, where its hydrogen-bonding and proton acceptor and donor sites provide diverse potential in both solid and liquid systems. In this work, imidazole is incorporated into a range of materials, including covalent organic frameworks, ionic liquids, and aqueous systems, to explore and deepen understanding of its unique properties and its role in material synthesis, thereby informing the future design of advanced proton-conducting materials.

Chapter 2

Proton exchange membrane fuel cells (PEMFCs)

Fuel cells are devices that harness energy from electrochemical reactions, by converting chemical energy into electrical energy. Put simply, a fuel cell is just an electrochemical cell in which the anode and cathode are spatially separated. Importantly, the sites of the two half-reactions are separated by an electrically insulating material, thereby forcing the electrons to follow a path through an external circuit and generate electricity. There are many different types of fuel cells, commonly categorized based on their electrolyte and choice of fuel. This thesis will focus on one of the most commonly discussed and implemented solutions, the proton exchange membrane fuel cell (PEMFC), and how it can be run on hydrogen. More precisely, the electrolyte in PEMFCs will be the overarching theme and application of this thesis, with synthesized materials explored as alternatives to the currently widely used proton exchange membranes.

2.1 Hydrogen as an energy carrier

As society phases out the use of fossil fuels, a new energy carrier will need to take its place. Part of the solution could be a transition to using hydrogen. In 2020, 98% of the global hydrogen production was still sourced from fossil fuels.[7] Produced hydrogen gas is classified based on the production method, the main ones being grey, blue, and green hydrogen. Gray hydrogen is made from hydrocarbons, mainly by steam reforming of methane, which makes up about three-fourths of the hydrogen produced. The transformation of methane and water to hydrogen also generates carbon dioxide (Equations 2.1 and 2.2), and the resulting hydrogen-carbon dioxide gas mixture is generally called syngas.[8] If no further steps are taken to manage the emissions of carbon dioxide, it will end up in the atmosphere, further warming the planet. If measures are taken to capture the carbon dioxide, such as through carbon capture and storage, the emissions will be significantly reduced, and the hydrogen produced is then

referred to as blue hydrogen.[9]

$$CH_4 + H_2O \longrightarrow CO + 3\,H_2 \tag{2.1}$$

$$CO + H_2O \longrightarrow CO_2 + H_2 \tag{2.2}$$

Another method of producing hydrogen is by electrolysis, which uses electricity to split water into hydrogen and oxygen (the opposite of the process used in a fuel cell, Equation 2.3).[7,10] This technology offers an excellent opportunity to produce hydrogen while also stabilizing the electricity grid. As the electricity grid becomes more dependent on variable energy sources, such as wind and solar power, it can experience significant fluctuations. When the grid has an excess of electricity, electrolyzers can be started quickly to produce hydrogen entirely from renewable energy sources.[11,12] The hydrogen can then be stored, for example, in tanks as liquid hydrogen, and subsequently used either to convert it back into electricity using a fuel cell when production is low, or for other purposes, such as steel production or production of chemicals. Electrolysis holds great promise: it is simple to implement, can generally be installed on-site and, when using renewable energy sources, the hydrogen produced has a minimal greenhouse gas footprint. This type of hydrogen is known as green hydrogen and lays the foundation for a possible hydrogen economy.[10]

$$H_2O \longrightarrow H_2 + \frac{1}{2}\,O_2 \tag{2.3}$$

Beyond its potential to balance the energy grid, hydrogen can also play a role in decarbonizing parts of the transport sector.[12] With transport responsible for about 16% of global greenhouse gas emissions in 2022, mobile applications of fuel cells have gained significant interest.[13] While battery-electric vehicles work well for cars, when long-range driving is considered, their weight quickly becomes an issue. Compared to other fuels, batteries have low gravimetric energy density, about 0.1–2 MJ/kg,[14] so while private short-range rides are easily accomplished, alternatives are needed for long-haul trucks, ships, and aircraft, where weight and recharge times become more important.[12] With hydrogen's much higher gravimetric energy density, about 120-140 MJ/kg,[15,16] it is a promising option for these applications. At the heart of these solutions lies the fuel cell.

There are multiple types of fuel cell technologies already established. Proton exchange membrane fuel cells, anion exchange membrane fuel cells (AEMFCs), alkaline fuel cells (AFCs), phosphoric acid fuel cells (PAFCs), solid oxide fuel cells (SOFCs), and direct methanol fuel cells (DMFCs), which all operate on the same principle but offer distinct advantages.[12] Table 2.1 shows some of the differences between these fuel cell technologies, such as operating temperature and niched applications.

Table 2.1: Common types of fuel cells with their operating conditions and some possible applications.[12,17–22]

Fuel cell type	**PEMFC**	**AEMFC**	**AFC**	**PAFC**	**MCFC**	**SOFC**
Electrolyte	Polymer	Polymer	KOH	Phospho -ric acid	Molten carbon- ate	Solid oxide or ceramic
Charge carrier	H^+	OH^-	OH^-	H^+	CO^{2-}	O^{2-}
Fuel	H_2	H_2	H_2	H_2	H_2, hydro- carbons	H_2, Hydro- carbons
Operating tem- perature (°C)	20–100	60–100	50–200	150–200	650	500–1000
Applications	Transport, backup power	Transport, backup power	Space vehicles	Integr -ated heat and power systems	Integr -ated heat and power systems	Integr -ated heat and power systems

2.2 Electrochemical reactions

Proton exchange membrane fuel cells are among the most researched and commercialized fuel cell options.[12] The typical operating temperature of current PEMFCs is 80 °C or below, hence they are generally classified as low-temperature proton exchange membrane fuel cells (LT-PEMFCs). This gives them an advantage in applications that necessitate short start-up times, such as fuel cell vehicles. PEMFCs are run on hydrogen as the fuel, which is allowed to react in a controlled way with oxygen, generally from ambient air. This reaction (Equation 2.4) is spontaneous and exothermic:

$$\mathrm{H_2} + \frac{1}{2}\,\mathrm{O_2} \longrightarrow \mathrm{H_2O} \tag{2.4}$$

The product, water, has a lower enthalpy than the reactants, hydrogen and oxygen, and it is this difference in energy that can be utilized. If allowed to react directly, all this energy is released as heat. To harness electrical energy the fuel cell is designed to spatially split the two half reactions. At the anode, the hydrogen oxidation reaction (HOR) splits hydrogen into protons and electrons (Equation 2.5).

$$\mathrm{H_2} \longrightarrow 2\,\mathrm{H^+} + 2\,\mathrm{e^-} \qquad E = 0.0\ V_{RHE} \tag{2.5}$$

Physically separated from the cathode, the electrons pass through an external circuit, producing an electric current, while the protons pass through a proton exchange membrane. At the cathode, they recombine with oxygen in the oxygen reduction reaction (ORR) (Equation 2.6).

$$2\,\mathrm{H^+} + 2\,\mathrm{e^-} + \frac{1}{2}\,\mathrm{O_2} \longrightarrow \mathrm{H_2O} \qquad E = 1.23\ V_{RHE} \tag{2.6}$$

Hence, utilising this simple reaction, in which the only product is water, the fuel cell can harness the energy released to supply electricity. Multiple components have been smartly designed and combined to leverage this beautifully

simple reaction; which will be discussed further in the following sections. A schematic of the flow and core components of the cell can be seen in Figure 2.1.

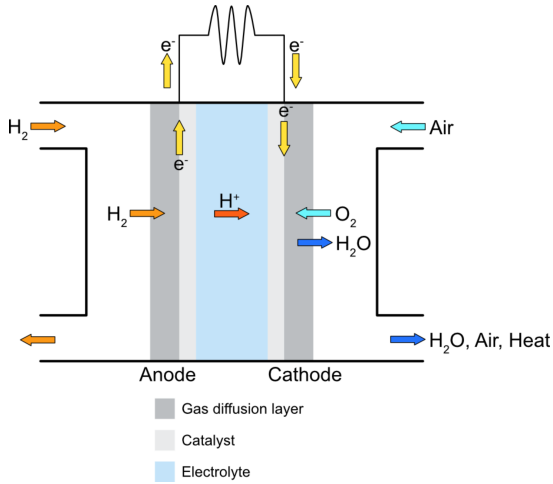

Figure 2.1: Schematic of a PEMFC, showing the flows through as well as the different parts of the cell.

2.3 Key components

A fuel cell based on a polymer electrolyte consists of five principal components.[22] At its core lies the proton exchange membrane (PEM), a solid polymer electrolyte that separates the two half-cell reactions, enables selective proton transport, and prevents electronic conduction. On either side of the membrane are the electrodes. This is where the half-cell reaction actually takes place, with the cathode and anode incorporating catalyst particles (generally platinum-based) supported on a porous structure (typically based on carbon). Therefore, they are commonly referred to as the catalyst layers. These three layers combined, anode, membrane, and cathode, are generally referred to as the catalyst-coated membrane (CCM). The CCM is flanked by gas diffusion layers (GDLs) on either side. These are porous, electronically conductive materials that facilitate uniform transport of reactant gases to the catalyst layers and efficient removal of reaction products (typically water). When combined, these parts, the membrane, catalyst layers, and gas diffusion layers, along with supporting gaskets, form a membrane electrode assembly (MEA). The MEA is the functional core of the fuel cell, and with all its layers, it is typically anywhere from 200-500 um thick. Finally, on either side of the MEA are the bipolar plates, which constitute the outermost layer. The bipolar plates serve multiple functions and provide the cell with stability. They can be further divided based on function into flow fields and current collectors. Adjacent to the GDLs are the flow fields, which distribute fuel to the anode and cathode on their respective sides of the cell and serve as the electrical contact between

the MEA and the current collectors. To achieve higher voltages than a single cell can provide, multiple cells are connected in series, forming a fuel cell stack. Here, the bipolar plates also act as interconnects, linking the anode of one cell to the cathode of the next, thereby enabling scalable power output.

2.4 Proton exchange membranes

The proton exchange membrane, sometimes also referred to as polymer electrolyte membrane, is the core of the fuel cell. Positioned between the anode and the cathode, its main function is to allow for efficient transport of protons. In addition to acting as a solid electrolyte, the PEM must possess other crucial properties.[12] First and foremost, it must be electrically insulating, ensuring that electrons are forced to travel through the external circuit to generate useful electrical current. Beyond physically separating the anode and cathode, the membrane must also prevent any crossover of reactants. If either hydrogen or oxygen gas leaks through the membrane, it would react directly, producing only heat rather than useful electricity. Furthermore, the PEM must withstand the harsh chemical and thermal environment within the fuel cell and be robust enough to endure the manufacturing process. Hence, a PEM needs to be an efficient proton conductor while having high electrical resistance, low gas permeability, and high chemical, thermal, and mechanical stability.[17]

As mentioned previously, PEMFCs are generally limited in operating temperature, working well at 80 °C and below. This is due to the specific chemistry of ionomers, which are a special family of polymers with ion-conducting properties, typically used as membrane materials. The most commonly used ionomer in PEMFCs, Nafion, was synthesized as early as 1960, but today there are multiple other derivatives available, such as GORE-SELECT, Flemion, and Hyflon.[17,18,23,24] These are all versions of perfluorinated sulfonic acid (PFSA) polymers with varying side-chain length and density, but they all share similar chemical structures and properties. Taking the widely used Nafion as an example, its chemical structure is shown in Figure 2.2. The backbone is polytetrafluoroethylene (PTFE), which is highly hydrophobic.[17,18] Moreover, the strong carbon-fluorine bonds endow the structure with high chemical stability, enabling it to withstand the highly acidic environment in the PEM. The backbone is decorated with side chains that terminate in sulfonic acid groups. The sulfonic acids are highly hydrophilic and can participate in the proton conduction of the membrane. These distinctly different sections of the polymer cause a characteristic phase-separated structure, with the backbone forming hydrophobic regions while the sulfonic acids aggregate into hydrophilic clusters. In its dry state, the proton conduction of Nafion is low, hence, it needs to be swelled with water. When exposed to water, the hydrophilic regions hydrate and swell and, if sufficiently swollen, form interconnected water channels throughout the polymer. Nafion can swell to absorb up to 50 % of its dry weight and exhibits a conductivity of 0.29 S cm^{-1}.[25]

To achieve high power density (i.e., a favorable power-to-volume ratio) and improved proton conductivity, there has been a trend toward thinner

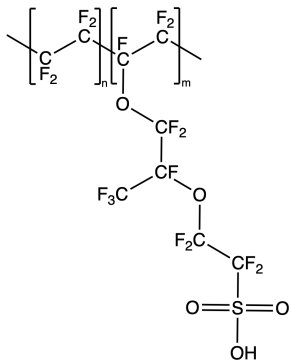

Figure 2.2: The chemical structure of Nafion™.

membranes.[12,18] However, this comes at the expense of reduced mechanical stability and an increased risk of hydrogen crossover. Due to their small size and high diffusivity, hydrogen molecules can permeate through thinner membranes, leading to voltage losses and accelerated membrane degradation. Consequently, a trade-off exists between enhanced proton conductivity and increased hydrogen permeability, which must be carefully considered when selecting the membrane thickness. Nafion membranes can be acquired in different thicknesses, with the current membranes being as thin as 15 μm.

To retain their proton-conducting properties, the commonly applied PFSA-based membranes need to be sufficiently swelled with water, the implication of which is a limited operating temperature to 80 °C or below. At increased temperatures the membrane readily dehydrates, and in doing so its proton conductive properties decrease by several orders of magnitude.[17] Hence, since the fuel cell generates heat while running, the whole system requires advanced cooling and water management solutions. Furthermore, these polymers lose their mechanical stability at elevated temperatures, with glass transition temperatures reported at 110-120 °C and relaxation of the side chains in Nafion at around 100 °C, leading to durability issues.[26,27]

An increased fuel cell temperature would not only reduce the need for cooling and water management but also improve kinetics and increase tolerance to CO poisoning. An improvement of the kinetics of the oxygen reduction reaction, which is typically the rate-limiting step and responsible for the majority of activation losses, would lead to higher cell efficiency.

There is one additional concern regarding the use of PFSA-based ionomers: the release of toxic chemicals.[17,28] More recently, per- and polyfluorinated alkyl substances (PFAS) have attracted growing scientific and political attention, and have in the process gained the name "forever chemicals". The same stability that makes them resistant to the temperature and acidic environment of the cell also means that if released, they are persistent and commonly bioaccumulative. While not an issue as long as they are confined to the fuel cell and handled correctly at their end of life, PFSA polymers still risk degradation. In fact, the polymer's main chain can be degraded through radical-initiated reactions.[17]

Given the reported toxicity and the increasing number of PFAS compounds being added to the Candidate List of Substances of Very High Concern under the REACH Regulation, there has been growing interest in replacing membranes with alternative, more sustainable materials.[28]

2.5 Benefits of higher temperature in PEMFCs

A shift to operation temperatures higher than 80 °C, targeting intermediate (80-120 °C) and high temperature (120-160 °C) PEMFCs, comes with quite a few advantages compared to low-temperature proton exchange membranes[29,30] The kinetics of both reactions improve, making it feasible to incorporate alternative, less expensive catalysts such as iron or cobalt, or decrease the platinum loading.[30–32] Furthermore, the impurity tolerance goes up, which can be exemplified by the CO tolerance increasing from 10-20 ppm to 1000 ppm when the temperature is increased from 80 °C to 100 °C. Decreasing the impurity limits means that lower-quality, cheaper hydrogen can be used, lowering the cost of running the cell. Increasing the operating temperature also simplifies the entire fuel cell system by reducing the need for water and cooling systems. As the operating temperature is raised above 100 °C, the water produced will be vapor, eliminating any problems related to electrode flooding. Furthermore, if intermediate-temperature proton exchange membranes wouldn't rely on water for proton conduction across the membrane, there would be no need for a humidifier, thereby removing it entirely from the system.

The solutions for reaching these intermediate and high temperatures can be divided into two major groups: the same PFSA polymers used in LT-PEMFCs, with modifications, and alternative polymer membranes, generally doped with acids.[30,33] The operating temperatures at which Nafion can be used and maintain high proton conductivity can be improved by introducing hydrophilic, generally inorganic, materials into the polymer to form a composite.[29,30] This strategy raises the operating temperatures to around 100 °C but still requires humidifiers. The option of swelling the polymer with alternative liquid electrolytes has also been explored, with ionic liquids being a promising option.[29] While there are a variety of alternative polymers available, the predominant choice and most researched options are polybenzimidazole (PBI) based polymers, doped with an acid.

There has been a variety of options developed that use acids as alternative liquid electrolytes, the most common of these being phosphoric acid (PA).[29,30] Phosphoric acid makes for a good liquid electrolyte in these applications due to its high proton conductivity under anhydrous conditions, low gas permeability, and good thermal and chemical stability.[34] Phosphoric acid was first explored in phosphoric acid fuel cells, in which the membrane was a PA-charged SiC matrix.[19] These fuel cells lost popularity, in part because the membrane required refilling due to the PA readily leaking from the cell. When using PA to attain intermediate- and high-temperature PEMs, the main difference is the matrix, with current solutions commonly being a polymer matrix, with a majority being PBI.[29,30] These matrices had clear advantages over the previous SiC matrices,

including easier handling, increased tolerance towards pressure differences across the cell, and decreased acid leaching.[34]

2.5.1 Polybenzimidazole membranes

There are a variety of structures available for polybenzimidazole polymers (one alternative in Figure 2.3), all being aromatic heterocyclic containing imidazole units, but their principal use of imidazole is the same.[34] The imidazoles, central to this thesis, can be protonated upon exposure to an acid, thereby gaining a positive charge. It is also this accepting, and subsequent giving, of a proton that allows the imidazole to participate in the proton conduction across the membrane. PA-doped PBI membranes can significantly increase the fuel cell's operating temperature, allowing it to operate well within 100-200 °C.[34,35] With PA responsible for the majority of proton conduction, high swelling of the membrane is generally desired. This, however, comes at a cost, as higher PA loadings are associated with lower mechanical stability. The mechanical strength of the PBI polymer is a result of close chain packing in the polymer, as the N and -NH- of the imidazoles form strong hydrogen bonds. At high acid doping levels, it begins to disrupt these bonds, separating the polymer backbones and reducing mechanical strength. To avoid this, PBI membranes can be reinforced by crosslinking or by incorporating PTFE polymers.[36,37] Moreover, increased temperatures also affect mechanical properties, with mechanical stability issues arising from creep deformation and acid leaching.[33]

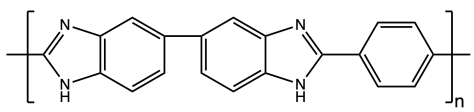

Figure 2.3: Chemical structure of the repeating unit in a PBI polymer.

Chapter 3

Alternative solid: covalent organic frameworks (COFs)

Having introduced the PEMFC technology, its possible role in phasing out fossil fuels, the components it is made up of, and how these limit its operation, this chapter will explore the first class of alternative materials proposed in this thesis: covalent organic frameworks (COFs). This chapter will delve into the chemistry and properties that make these structures intriguing, and show examples of how they can be employed as solid electrolytes in PEMFCs.

Polymers comprise a significant portion of the materials we interact with daily, from our clothes to our lunchbox, including natural fibers like cellulose and synthetic plastics like polyesters and nylon. The basic understanding of polymer structures has been established for a century, but it is only more recently that researchers have gained the necessary understanding of how to create long-range order in these materials, forming precisely designed architectures on a nanometer scale.

COFs are a subgroup of traditional organic polymers. To make conventional organic polymers porous, organic building blocks can be randomly interconnected through covalent bonds to form accessible voids, resulting in materials that are generally referred to as porous polymer frameworks (PPFs) or porous organic polymers (POPs). However, this does not allow for the control of the size or shape of the voids as the chains intertwine to form an amorphous mass. COFs, however, utilize pre-designed organic building blocks to control their behavior, thereby achieving long-range order. This was first achieved in 2005 by Omar M. Yaghi, who synthesized a highly ordered 2D organic polymer based entirely on covalent bonds.[38] The 2D sheets, formed by the self-condensation of boronic acids to produce boroxine anhydride-based linkages (B_3O_3 rings), stack on top of one another due to intermolecular forces to form the framework structure of COF-1. While being a significant breakthrough for modern polymer science, the fairly unstable boron linkages used in early COFs were overtaken by C-N bonds in 2009 with the synthesis of COF-300, which have since been the predominant bond in COF synthesis.[39] The increased stability, permanent

porosity, and the possibility of incorporating a wide variety of functionalities have since made COFs gather interest in a wide range of applications, such as gas adsorption,[40] separation,[41] sensors,[42–44] water treatment,[45] proton conduction,[46] organic electrodes,[47] heterogeneous catalysis,[48–50] optoelectronics,[51] and semiconductive materials.[52] To better design these materials for such applications, one must first grasp the fundamental principles and underlying concepts of their design and synthesis.

3.1 Reticular chemistry and topology

The conceptualization and realization of the first porous framework materials were achieved not through the covalent bonding that defines covalent organic frameworks (COFs), but rather through the coordination bonds characteristic of metal–organic frameworks (MOFs). These materials laid the foundation for the field of reticular chemistry, which, as defined by Yaghi, is the chemistry of linking molecular building units by strong bonds into predetermined, ordered structures.[53] This enables the rational design of extended frameworks, where structures are constructed through the deliberate selection of geometrically and chemically compatible building units, rather than through trial-and-error or serendipitous discovery.

Central to reticular chemistry is the abstraction of complex structures into simpler building blocks and their modes of connection. In this framework, geometry and connectivity serve as the guiding principles, formalized through the concept of topology.[54] Rather than treating molecular building units in terms of their full atomic detail, topology reduces structures to their essential connectivity and symmetry. In this representation, atoms or clusters are treated as vertices and the bonds between them as edges, forming a periodic net. Importantly, this abstraction allows chemically distinct materials to be classified within the same topological family, provided they share the same underlying connectivity and spatial arrangement.

This mode of structural abstraction originates from the work of Arthur D. Wells,[55] who introduced the use of nets to describe and visualize crystalline solids. His approach has since been significantly expanded and formalized within reticular chemistry.[54] As the field grew, the need for a standardized nomenclature became apparent. Yaghi and co-workers addressed this by introducing a systematic labeling for crystal nets consisting of a three-letter lowercase combination, e.g., *pcu*, *dia*, *hcb*.[56] In parallel, the Reticular Chemistry Structure Resource (RCSR) database was established, providing a comprehensive repository of known topologies, including detailed information on their symmetry, vertex connectivity, and edge relationships.

Periodic nets can be understood as a specialized class of graphs.[54] While they share similarities with graph theory in mathematics, the concept as employed in reticular chemistry differs in its emphasis and application, and the two should not be conflated. In this chemical context, topology encompasses all symmetry, preserving transformations of a structure, such as stretching, bending, or distortion, so long as the connectivity between vertices remains

unchanged. Thus, topology does not explicitly consider bond lengths and angles; instead, these geometric parameters may vary within chemically reasonable limits while preserving the underlying network connectivity. In translating these ideas to chemical structures, vertices corresponding to atoms, metal clusters, or molecular building units, while edges represent the bonds connecting them, this abstraction enables a direct link between molecular design and extended structure.

When designing a COF with a targeted topology, several factors must be carefully considered. Once a desired net has been selected, it can be deconstructed into its constituent geometric building units, for which connectivity and angular relationships are critical.[54,57] These geometric constraints must be matched by the chosen molecular precursors to ensure that the assembly yields the intended topology, rather than an alternative network accessible from the same components. Although not universally applicable, COF structures are often described in terms of nodes and linkers, with nodes typically possessing higher connectivity and acting as the vertices of the network, while linkers are commonly ditopic, approximately linear units that bridge nodes and define the edges of the structure. For 2D structures, only a handful of topologies have been realized, though they can be constructed from different building blocks, some of which are in Figure 3.1).

3.2 Dimensionality of COFs

Closely related to the underlying topology of the framework, COFs are commonly classified into three categories based on their dimensionality: 3D, 2D, and 1D. This classification reflects the number of spatial directions along which covalent bonding extends throughout the framework.[57] In 3D COFs, covalent bonds propagate in all three spatial directions, resulting in fully interconnected networks. Common topologies observed in 3D COFs include *dia*, *pts*, and *bor*. In contrast, in 2D COFs covalent bonding extends within the plane, forming extended sheet-like layers.[58,59] These layers stack, being held together by weaker non-covalent interactions, such as π–π stacking and van der Waals forces. This anisotropic bonding often leads to layered materials with directional properties.[54] 1D COFs are less common and consist of covalent bonding nets along a single spatial direction, forming chain-like structures. Despite their one-dimensional connectivity, they differ from conventional linear polymers in that their structures are typically designed with periodicity and may exhibit accessible porosity and/or well-defined geometries along the chain. Structures with zero-dimensional (0D) connectivity do not form extended frameworks, as there is no continuous bonding between repeating units. Instead, such systems correspond to discrete entities such as cages or macrocycles, which may still possess internal cavities but do not belong to the reticular material family.

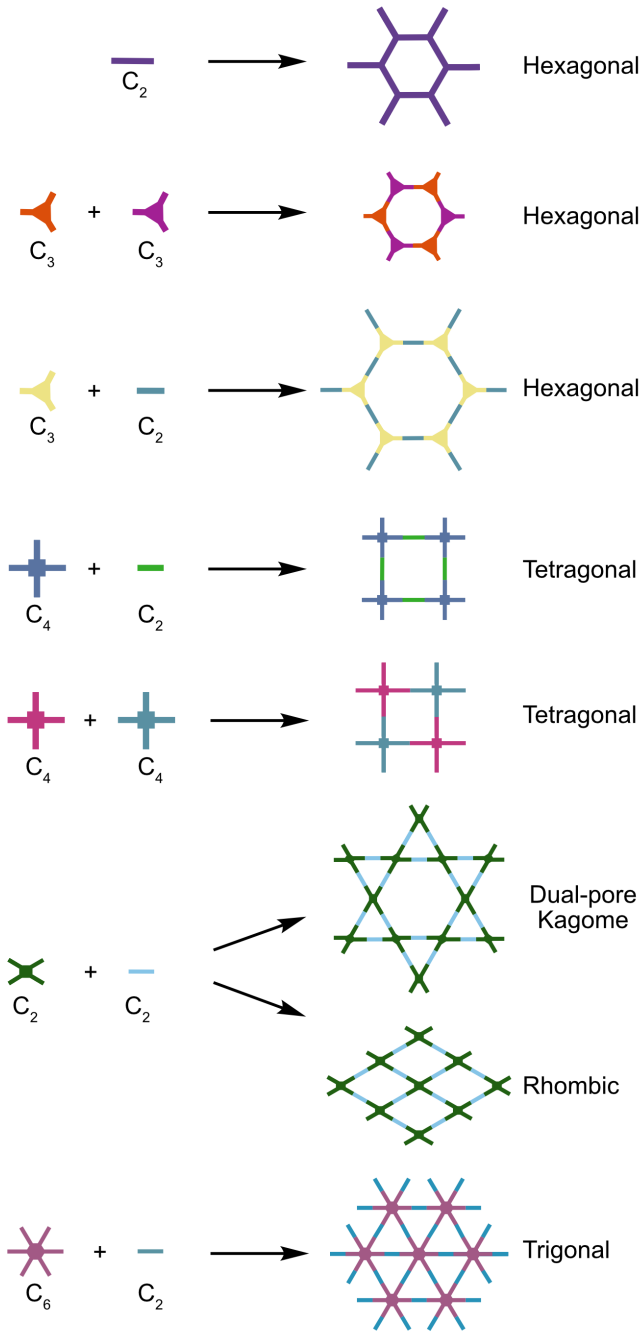

Figure 3.1: Some of the 2D structures in COFs illustrated as their basic geometric building blocks and resulting pores.

3.3 Powders, films and crystals

The way in which COFs are synthesized has a drastic effect on the types of materials obtained. Most commonly, COFs are made by solvothermal synthesis, with the product formed being polycrystalline powders.[57,60] The standard procedure, used for the first COFs[38] and still the predominant method, is the following: the precursors are added to a tube, with solvent (most commonly a mixture of dioxane and mesitylene or o-dichlorobenzene and butanol, but will occasionally also include NMP, THF, or other organic solvent), and a small amount of acid catalyst (generally acetic acid at three or six molar concentrations). With the reagents most commonly dissolved at this stage, sometimes with the help of sonication, the tube is then subjected to three freeze-pump-thaw cycles, after which it is flame-sealed and heated to 120 °C for 3-7 days. This results in a powder, which is then subjected to washing in some form, either by filtration, centrifugation or, for the most rigorous option, Soxhlet extraction. After this, the powders are collected and dried, usually at elevated temperatures and reduced pressures, for activation.

While this synthesis is relatively straightforward on a small scale, it presents clear limitations to upscaling and practical applications. Although the resulting powders can be pressed into pellets or incorporated into composite materials, forming a robust, continuous solid remains challenging, as the particles are neither readily fusible nor soluble. Furthermore, due to their polycrystalline nature, the individual particles contain grain boundaries. These may appear as well-defined interfaces between crystalline domains or as thin amorphous regions linking adjacent crystallites. Moreover, the prevalence of these grain boundaries is influenced by the crystallite size. Such structural features can significantly affect transport properties within the material. For example, grain boundaries may disrupt pore connectivity, leading to discontinuities that hinder mass transport.

To improve the crystallinity of COFs and enable more precise structural characterization, significant research efforts in recent years have focused on the synthesis of single-crystalline COFs. This development has been especially impactful, as single-crystal X-ray diffraction (SCXRD) provides substantially higher structural resolution than powder X-ray diffraction (PXRD), enabling unambiguous determination of atomic positions and clear differentiation of diffraction features that may otherwise overlap in PXRD patterns.[61] The ability to obtain single crystals has therefore enabled a deeper understanding of COF topology, stacking behavior, pore architecture, and the presence of structural defects.[62] In contrast to polycrystalline samples, where peak broadening, preferred orientation, and structural disorder can complicate analysis, single-crystal studies provide direct insight into framework symmetry, interlayer interactions, and subtle structural distortions.

Considerable progress has been made in the synthesis of single-crystalline COFs. Early reports often required weeks to months to grow relatively small crystals, reflecting the inherent challenges of balancing reversible bond formation with controlled nucleation and growth.[63] More recently, improved synthetic strategies have enabled faster crystallization and the formation of larger, higher-

quality crystals. These advances are largely based on a deeper understanding of the underlying reaction kinetics, particularly the role of solvent systems, concentration, temperature, and the use of modulators.[64] Solvent choice plays a critical role in controlling solubility, diffusion, and reversibility of bond formation, while modulators can regulate nucleation rates and promote defect healing by slowing down framework formation.[61] Such approaches allow for more controlled crystal growth, hence improving crystallinity and enabling single-crystal formation. These strategies will be discussed in greater detail later in this chapter.

The third typical form that COFs are made in is films, while these can be accomplished using a handful of different methods, they can be divided into top-down or bottom-up approaches. Top-down approaches use pre-synthesized 2D frameworks and aim to break the interlayer forces to separate the sheets. This can, for example, be done by grinding[65] or sonication,[66] breaking the sheets into stacks of 3-30 layers depending on the method and COF used. Sheets can also be separated by chemical exfoliation, generally using steric effects introduced by bulky substituents to overcome attractive interlayer interactions.[67] Examples have also been shown in which self-exfoliation can be induced, for example, by ionic effects.[68] The sheets can then be cast into a continuous film.

Bottom-up approaches grow the COF as a film. This is commonly done by containing the reaction to an interface, either air-liquid,[69] vapor-solid,[70] liquid-solid[71] or liquid-liquid.[72] Another approach is to dropcast the reaction mixture onto the substrate and then have the reaction take place, for example, by vapor-assisted conversion.[73] COF films can also be grown on conductive templates by electrophoretic deposition, utilizing the intrinsic electric surface charge of COFs immersed in a non-conductive solvent.

3.4 Crystallization behavior

The exact crystallization mechanism of COFs is not yet fully understood; however, different conceptual models have been proposed to describe their formation. Based on the impact of reversibility and thermodynamic control, one hypothesis is that the COFs initially form as amorphous polymer networks through rapid chain-growth polymerization.[74] Subsequent error correction, enabled by reversible bond formation, allows the system to reorganize toward a more ordered, thermodynamically favored crystalline structure. Controlling monomer solubility and reaction kinetics is therefore critical, as it slows down nucleation and promotes defect healing. Within this framework, additional non-covalent interactions, such as π-π stacking, are thought to further stabilize the emerging crystalline order. However, the successful synthesis of highly crystalline COFs via irreversible linkages challenges the universality of this mechanism, suggesting that long-range order can be achieved even in the absence of dynamic covalent error correction. As a result, an alternative model based on the preorganization of reactants has been hypothesized.

In the preorganization-driven mechanism, the sequence of events is effectively reversed. Rather than forming a disordered network first, the molecular building

blocks are thought to assemble into ordered or semi-ordered arrangements through favorable non-covalent interactions, such as π-π stacking, hydrogen bonding, or solvophobic effects, prior to and during covalent bond formation.[75] Polymerization proceeds within this preorganized environment, leading to the gradual formation of extended, initially disordered sheets that can undergo further structural rearrangement into well-defined crystalline frameworks.

When attempting to push crystallization toward the formation of single-crystalline COFs, both of the proposed mechanisms highlight the importance of carefully controlling reaction conditions. In particular, solvent choice and the solubility of linkers and intermediate oligomers play a crucial role in modulating nucleation and growth kinetics.[64,76] At the same time, promoting effective preorganization of the building blocks has been shown to be equally important for achieving high crystallinity and large crystal domains. Furthermore, the solvent mixture matters, with solvent structuring in one of the most commonly used systems (dioxane/mesitylene/acetic acid) having been shown to accelerate polymerization and nucleation by acting as a kinetic modulator.[77]

Furthermore, an alternative study using ultrasmall-angle X-ray scattering (USAXS), has suggested that single crystals of imine linked 2D COFs are formed by the fusion of small hexagonal platelets into fractal like intermediates, which form clearer facets and develop into larger hexagonal crystals.[64] When instead using conditions to form polycrystalline powders of the same structure, their particle growth included the formation of aggregates. Moreover, another study proposed that 2D COFs first form disordered sheets, which through structural rearrangement form the final stacked COF structure.[78] Furthermore, in situ measurements using dynamic light scattering and liquid cell transmission electron microscopy have been employed to investigate the formation of imine-linked COF nanoparticles, in which three stages of the formation could be identified: nucleation, growth, and ripening.[79]

3.4.1 Nucleation and growth

A key aspect in understanding COF crystallization is the interplay between nucleation and crystal growth, as these processes ultimately determine crystal size, morphology, and degree of order. In general, and in accordance with the LaMer mechanism,[80] nucleation refers to the initial formation of stable molecular clusters (nuclei), while growth describes the subsequent addition of building blocks to these nuclei to form extended crystalline domains. In many COF systems, crystallization is thought to be strongly nucleation-controlled. This has been exemplified in studies of COF-5, which show, by simulation and experimental results, that there is a first-order growth and second-order nucleation dependence on monomer concentration.[81] To limit nucleation and instead favor the growth of large crystals, a monomer concentration, C^*, was proposed. C^* is linearly dependent on existing nuclei and is the concentration at which the fastest crystal growth is achieved. As it is hard to maintain a constant monomer concentration, it was instead suggested to make slow additions of monomer solution to the reaction mixture, thereby growing fewer, larger crystals. The choice of solvent during COF-5 synthesis has also been

proposed to significantly affect crystallization behavior in theoretical studies.[82] With solvent choice affecting stacking interactions, a decrease in stacking interactions led to an increase in crystallite size. This was due to an increased nucleation free-energy barrier and more frequent dissociation of defective aggregates, allowing annealing of COF-5 fragments. This, however, seems to contradict certain aspects of the suggested COF growth via supramolecular preorganization.

3.4.2 Impact of reversibility

Dynamic covalent chemistry (DCC) is based on reversible reactions operating under thermodynamic control.[83] This enables the system to avoid kinetic traps and instead equilibrate toward the lowest-energy state, which in the case of COFs corresponds to their crystalline state. While reversible chemistries have been extensively employed to access highly crystalline products, the underlying mechanisms that govern error correction and how it influences the product, forming single crystals, polycrystals, or amorphous solids, are not yet well understood. Theoretical studies have suggested that the bonding energy, as described by the Arrhenius two-state model for reversible reactions, can be correlated to the product formed.[84] It suggests that single crystals can be formed by highly reversible reactions (low bonding energies) during ultra-slow growth, as this inhibits nucleation and corrects defects through the continuous removal of defective fragments at the crystal edges. High bonding energies, on the other hand, corresponded to high nucleation rates and rapid growth. The rapid growth incorporated defects into the crystals, which, during the defect-correction process, caused the crystals to divide, yielding smaller crystals and polycrystalline materials.

3.4.3 Stacking in 2D COFs

Owing to the weak non-covalent interactions between layers, 2D COFs can adopt a variety of stacking configurations that are often close in energy but give rise to distinct physico-chemical properties in the corresponding 3D material. These stacking arrangements can be described using two primary structural parameters: the lateral displacement in the xy-plane, referred to as interlayer slipping (ILS), and the interlayer separation along the z-direction, known as the interlayer distance (ILD) (Figure 3.2). In the absence of lateral displacement, where layers align directly on top of one another, the structure is classified as AA-stacked. In contrast, AB-stacking corresponds to the maximal lateral offset, in which the vertices of one layer are positioned above the pore centres of an adjacent layer. A continuum of intermediate configurations exists between these two cases, arising from partial interlayer displacement. Depending on the degree and nature of long-range order within the multilayer assembly, these partially offset structures can be categorized as inclined (unidirectional slipping), serrated (alternating slipping), or random; the latter representing a combination of inclined and serrated motifs.

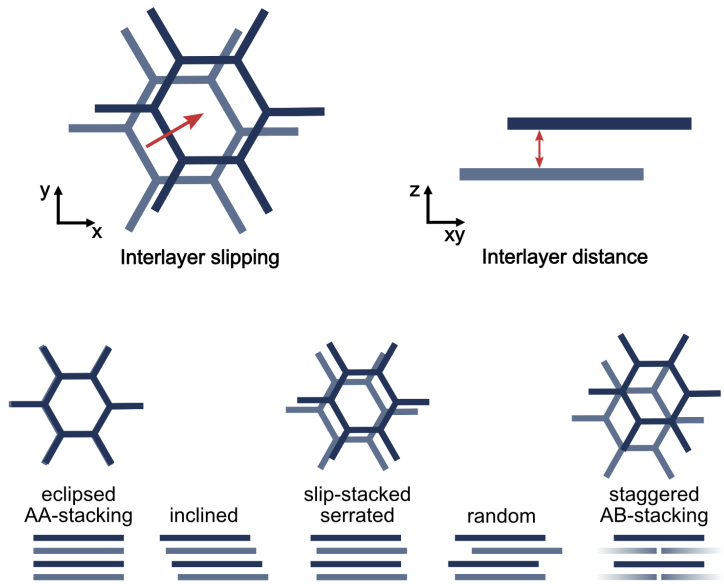

Figure 3.2: Examples of stacking patterns in 2D COFs.

3.5 Linkages

The earliest realized COF chemistries were based on reversible reactions, boronic acid trimerization,[38] boronate ester formation,[38] trimerization of nitriles,[85] and the Schiff base reaction.[39] Since then, the available linkage chemistries has rapidly increased, with irreversible bonds such as olefins,[86–88] sp^2 carbons,[89,90] phenazines,[91] dioxines,[92–94] oxazoles,[95,96] thiazoles,[95,97] polyphenylenes,[98] and nitrones[99] all being realized. Some common linkages and their reactants can be seen in Figure 3.3.

Cascade reactions have offered a possible route to irreversible bonds. By combining the formation of reversible linkages with a subsequent irreversible step, this approach can allow for the thermodynamic reversibility that is necessary to reach crystallinity while affording the kinetically stable product. A typical example of this is the keto-enamine tautomerization, first utilized in 2012.[100] By utilizing the same Schiff base reaction commonly used in COFs, they could achieve crystallinity, but by installation of a hydroxyl group on the benzene node, the structure could undergo an irreversible tautomerization from the enol to the keto form. This drastically enhanced the stability compared to other COFs available at that time, being stable in both acid, bases, and boiling water.

3.5.1 Imine linkage

The imine linkage is currently the predominant linkage chemistry in COFs. Having been reported by Schiff as early as 1864, the reaction itself is fairly

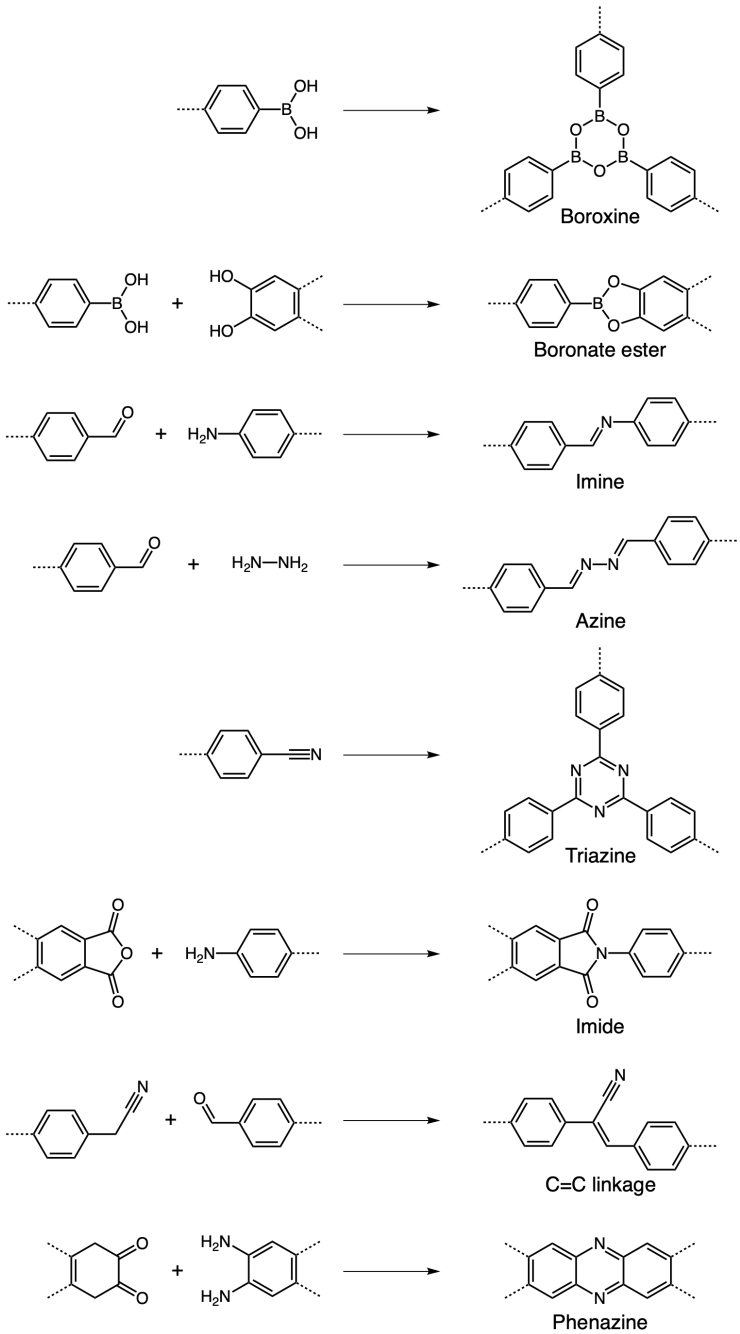

Figure 3.3: Commonly used linkages in COFs and the groups that they are formed by.

straightforward.[101] A carbonyl compound and an amine react by nucleophilic addition to give a hemiaminal intermediate, which, upon the elimination of water, forms the imine (Figure 3.6). This reaction is reversible, and the equilibrium can be influenced by concentration, steric and electronic effects, pH, temperature, catalyst choice, and solvents.[102] Lewis acids can be used to catalyze the reaction, catalyzing the nucleophilic attack of the amine on the carbonyl group while also acting as a dehydrating agent through irreversible binding with water to promote the final step.

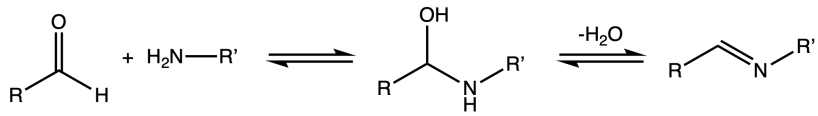

Figure 3.4: Schematic of the Schiff base reaction, forming an imine by the reaction of an aldehyde with an amine.

When using the imine condensation reaction to form COFs, the water content has a substantial impact. Systematic studies suggest that adding water favors the backreaction and that increasing the amount can improve crystallinity.[74] Addition of acetic acid to the reaction, without the addition of water, causes a fast forward reaction and the formation of amorphous polymers. To obtain a crystalline material, a sufficient amount of water must be introduced, indicating that the water generated during the condensation reaction is insufficient to promote the reverse reaction to the extent needed to achieve the dynamic correction of the framework.

3.5.2 Imidazole linkage

The imidazole linkage can be considered irreversible, as once the heterocycle is formed and oxidized into the imidazole, it can not readily be reversed. To form robust linkages, the Debus-Radziszewski multicomponent reaction was used to synthesize imidazole-linked COFs.[103] While first applied to 2D COFs, it has since been extended to 3D structures as well.[104] Previously, the polyphosphoric acid-catalyzed reaction of aryl carboxylic acids with o-diamines has been used to form imidazole-linked 2D COFs.[105] This has also been attempted to form 2D COFs of hexagonal pores, but yielded very limited crystallinity.[106] Imidazoles can also be formed by a cascade reaction of o-diamines and aldehydes, which will be explored later in this thesis.

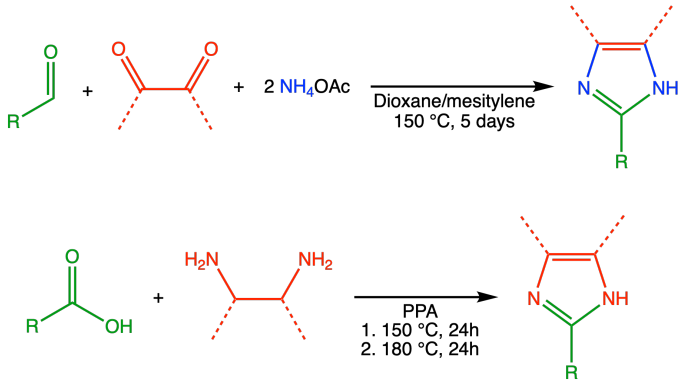

Figure 3.5: Schematic of two common imidazole-forming reactions; the Debus-Radziszewski multicomponent reaction (top)[103] and the polyphosphoric acid-catalyzed reaction of aryl carboxylic acids with o-diamines (bottom).[105]

3.6 Modulators

The use of modulators in the formation of framework structures was first introduced during MOF synthesis.[107–109] Mono-functionalized terminating ligands were added to the synthesis, competing with the symmetric bridging ligands for coordination to the metal of the MOF. Following an improved understanding of crystallization behavior, as discussed in Chapter 3.4, this strategy was subsequently extended to COFs. The first modulators were used during the synthesis of COF-5, using either 4-tert-butylcatechol (TCAT) or 4-mercaptophenylboronic acid.[110,111] It could be shown that the addition of a modulator slowed down the formation of the framework, enabling the growth of larger crystalline domains. Moreover, when using TCAT, the use of TCAT resulted in high yields with little to no incorporation of the modulator into the final product.[110] From this, they could conclude that there was a driving force towards COF formation, and thereby hypothesized that an irreversible process occurred downstream of the initial covalent bond formation. In contrast, when monoboronic acid modulators were used, they were incorporated into the COF structures but localized to the grain boundaries.[111] Based on these observations, it was proposed that such modulators slow down the reaction by reversibly binding to and dissociating from the edges of the growing two-dimensional sheets, facilitating defect healing and promoting the formation of larger crystallites.

Modulators were also the key to unlocking large imine-linked COF single crystals.[61] By the addition of a large excess of aniline and long reaction times (up to 80 days), micrometer-sized high-quality crystals of 3D COFs could be obtained and studied by single crystal X-ray diffraction. A systematic screening of substituted aniline derivatives revealed that the reactivity of the modulator plays a critical role in the crystallization process. In particular, a mismatch between the reactivity of the amine building block and that of the modulator resulted in products with reduced crystallinity or, in some cases, complete

suppression of framework formation. Aniline has since become a widely used modulator in many COF systems, promoting higher crystallinity. More recently, aniline dosage has also been used as a tool to control the morphology of single crystals.[112]

Different modulators can also be used in combination, as exemplified by the simultaneous use of benzaldehyde and aniline to alter COF morphology.[113] Notably, in contrast to the amorphous-to-crystalline formation of other unmodulated imine COF synthesizes,[74] this approach generated crystalline products at the initial stage of the reaction that then grew with reaction time.

With thoughtful selection and optimization, modulators have become an indispensable tool in controlling COF synthesis, offering a means to control crystallization, achieve larger crystal domains, amplify surface area, and refine pore distribution.[114]

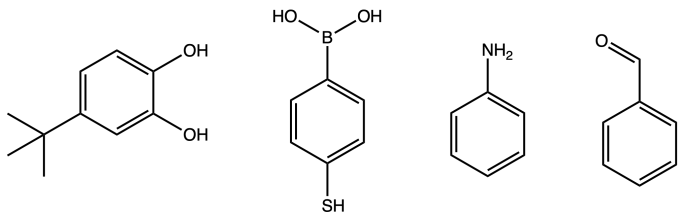

Figure 3.6: Molecular structures of some of the modulators used during COF synthesis; from left to right: 4-tert-butylcatechol, 4-mercaptophenylboronic acid, aniline, and benzaldehyde.

3.7 Linker-exchange

Linker-exchange has had numerous applications in the formation of COFs, including altering the structure and dimensions,[115] changing pore size,[116] achieving otherwise unattainable structures,[117] and utilizing COPs to convert them into COFs.[118] In short, the method is based on the replacement of one of the parts of the COF, using the reversibility of the original bond and extra equivalence of the alternative linker to take its place. In doing this, the structure is already pre-formed, with all the bonds being in the right place, similar to pre-assembly, but with already formed bonds making up the structure. If done with the right kinetics, the linkers can be switched out at a speed that preserves the structure's integrity, with an alternative piece taking its place. This can also be done to achieve otherwise hard-to-attain structures with irreversible bonds. This was, for example, done by Yaghi et al.,[119] where an imine-bonded linker was substituted for one forming oxazole and thiazole bonds. When forming the heterocyclic rings, the pre-network was treated with 4-8 equivalents of the new linker. The new linker would take its place, first forming an imine bond but then reacting further through cyclization and dehydrogenation to reach the final structure. They encountered one problem: the dehydrogenation could lead to the hydrogenation of nearby imines, resulting in the formation of

irreversible amine bonds and hence a mixture of linkages in the final product. To limit this side reaction, the reaction was carried out under oxygen, which could oxidize the cyclic intermediate and minimize the formation of any amines. This reaction, as well as the method, is similar to aspects explored in the results of this thesis.

3.8 COFs for proton conduction

Testing COFs for proton conduction and their application in PEMFCs arose as a natural response to the porosity and diversity that COFs offer, and has since gained more traction.[120] COFs offer the option of combining intrinsic and extrinsic proton conduction by installing proton-conduction groups in the COFs and filling the porous structure, respectively.

Attempts to do so were made as early as 2016, using sulphonic acid group-containing linkers and charging the pores with phytic acid.[121] In 2019, the NKCOFs 1-4 series further explored how COFs can combine intrinsic and extrinsic proton conduction.[122] To do this, a stepwise synthesis strategy was applied, making it possible to install both azo and phenolic hydroxyl groups, allowing for binding of an external proton conductor and intrinsic proton conduction respectively. By loading the porous structures with H_3PO_4, a proton conduction of 1.13 10^{-1} S cm^{-1} could be achived at 80 °C and 98% RH. Furthermore, when included in a MEA, a maximum power density of 81 mW cm^{-2} and a maximum current density of 456 mA cm^{-2} could be obtained. As PA provides high proton conductivity, it has since been applied in many more COFs.[46,123]

When the 1D channels of the olefin-linked pyrazine COF, NKCOF-10, were charged with PA it afforded high proton conductivity, 9.04 10^{-2} Scm^{-1}, and ultralow activation energy, 0.06 eV. The nitrogen in the pyrazine linkers was exploited to confine and stabilize the PA, anchoring it and enhancing proton hopping. By combining H_3PO_4@NKCOF-10 with 3 wt% PTFE, a realistic proton exchange membrane could be formed, and when tested in a fuel cell, reach power and current densities up to 135 mW cm^{-2} and 676 mA cm^{-2}.

Similar to PBI membranes, imidazole-linked COFs charged with PA have shown good proton-conductive capabilities.[105,106] More precisely, H_3PO_4@PBI-COF had a proton conduction of 1.57 10^{-1} S cm^{-1}, and when supported by 4 wt% PTFE and applied in a MEA reaching up to 0.936 V open-circuit voltages and 125 mW cm^{-2} maximum power densities. Sulfonic acid groups have also been shown to have a positive effect on H_3PO_4 doped COFs.[124] By intrinsic surface sulfonation of PyHATP-1 the H_3PO_4@PyHATP-1-SO_3H had a higher proton conduction than its non-functionalizaed counterpart by almost two orders of magnitude, a value of 0.88 10^{-1} Scm^{-1}.

By charging a variety of COFs with PA, it was shown that increasing pore size decreases the activation energy barrier for proton conduction, with a linear dependence.[46] It was also shown that the proton conduction in micropores was governed by sluggish vehicular conduction, while the larger mesopores enable fast proton hopping across the channels, reaching a proton conductivity of 0.31

S cm^{-1}.

Further, Yu Fu et al. reported a series of zwitterionic COFs, XJCOF-1, XJCOF-2, and XJCOF-3, which were charged with either 1,2,4-triazole or imidazole to achieve proton conductivities of 4.3-12.9 10^{-3} S/cm (150-160 °C) and 2.43-4.38 10^{-2} S/cm (140 °C), respectively.[125] This corresponds to a proton conductivity that is higher than that of neat imidazole/triazole melts and an E_a similar to that found in hydrated Nafion.

Careful design of the pore surface and shape has been explored for enhanced proton conduction, engineering concave dodecagonal nanopores embelished with functional groups, which once loaded with PA reached a proton conduction of 2.33 10^{-2} S/cm and worked well in a wide temperature range of 80-160 °C.[126]

Anhydrous proton conduction has been achieved in sulphonic acid-grafted COFs by charging them with ionic liquids, reaching 2.21 10^{-3} S cm^{-1}.[127] A struturing effect has been seen when charging COFs with ionic liquids, adopting a layered structure, alternating cations and anions, due to stronger interactions between cations/anions and the pore wall.[128]

Furthermore, the rigid channels of COFs have been shown to improve proton conduction at low relative humidity compared to conventional Nafion membranes.[129] The synthesized IPC-COF membranes had improved water retention and hence showed weakly humidity-dependent conductivity in broad RH ranges (30–98 %). This can be rationalized by the pore structures of either membrane, with the amorphous soft channels of polymer membranes going from open at high relative humidity to isolated clusters or mostly dried-out connected channels upon decreasing relative humidity. COFs, on the other hand, preserve their channel diameter even at lower relative humidity, and the strong capillary effect within the crystalline, rigid nanochannels makes them retain water molecules more effectively. Hence, the ICP-COF membranes exhibited an unprecedented proton conductivity that was 1–2 orders of magnitude higher than that of benchmark PEMs at low RH (30%).

Chapter 4

Alternative liquid: protic ionic liquids (PILs) and aqueous imidazole

Having introduced an alternative solid electrolyte, COFs, this chapter will turn the focus towards the liquid electrolyte. As discussed previously, the most common PEMs based on PFSA polymer membranes are usually swelled with water to achieve high proton conductivities, but there exist other options to consider. PBI-based membranes and many of the COF alternatives presented in the previous chapter have been charged with PA to achieve good proton-conduction properties under anhydrous conditions. Here we delve into two suggested alternatives: protic ionic liquids (PILs) and aqueous imidazole.

4.1 Proton transport mechanisms

Proton conduction is a fundamental process in many systems and is essential for fuel cell operation. In contrast to regular ion transport, in which ions move by diffusion as individual units, hydrogen can also participate in an alternative mechanism, structural diffusion.[130] While protons are usually associated to a host, they can, based on the dynamic character of hydrogen bonds, also move between molecules. Hence, there are two modes of proton transport: the vehicular mechanism,[131] governed by self-diffusion, and the proton-hopping mechanism, which shuttles protons between molecules faster than the parent molecules themselves. Proton hopping is considered more efficient because it does not require movement of the whole molecule.[130] This is reflected in a lower activation energy, with systems dominated by the proton hopping mechanism correlated with $E_a < 0.4$ eV, and values above this indicative of systems governed by the vehicular mechanism. The proton-hopping mechanism is commonly observed in systems with high proton conductivity, such as water[132] and PA,[133] but has also been reported occasionally in protic ionic liquids.[134,135]

These transport properties arise from the balance between attractive and

repulsive intermolecular interactions. Consequently, they exhibit a strong dependence on temperature, as increasing thermal energy weakens these interactions. The relationship between temperature and ionic conductivity (or viscosity) can be described by the Vogel–Fulcher–Tammann equation,

$$\sigma = \sigma_0 \cdot e^{(-\frac{DT_0}{T-T_0})} \tag{4.1}$$

in which σ_0 is the ionic conductivity extrapolated for infinite temperatures, D is the strength parameter (which, for ionic liquids, can be related to the system's fragility), T is the absolute temperature in Kelvin, and T_0 is the Vogel temperature. Several approaches can be used to represent the relationship between conductivity and temperature, the most common ones being the use of Arrhenius and Angell plots. In the Arrhenius plot the logarithm of conductivity, $ln\sigma$, is plotted against inverse temperature, $1/T$, whilst in the Angell plot a T_g-scaled temperature axis is used.

4.2 Protic ionic liquids

Over a century ago, Paul Walden synthesized the first room temperature ionic liquid, ethylammonium nitrate (Figure 4.1), marking the start of what would become a field of nontraditional solvents.[136] Walden attributed its unusually low melting point (13–14 °C) to a reduced extent of ion association, arising from the large organic cation.

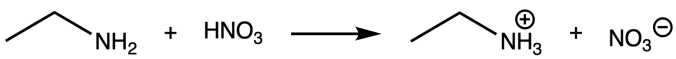

Figure 4.1: The acid-base neutralization reaction between ethylamine and nitric acid to form ethylammonium nitrate.

Typically, ionic liquids (ILs) are defined as salts with melting points below 100 °C, whereas salts with higher melting points are classified as molten salts.[136] In addition to their low melting points, ILs are generally characterized by negligible vapor pressure, low flammability, strong solvating ability, and favorable thermochemical and electrochemical properties. ILs can be broadly divided into two main classes: protic and aprotic. Although they share many features, their synthetic approaches differ and the presence of a transferable acidic proton in protic ionic liquids (PILs) can lead to behavior that deviates from that typically observed in aprotic ionic liquids (AILs).

AILs and PILs are synthesized by different reactions (Figure 4.2). AILs are commonly formed by quaternization reactions of amines with alkyl halides. The analogous PILs are formed by an acid-base neutralization reaction, transferring a proton from a Brønsted acid to a Brønsted base,

$$\mathrm{B} + \mathrm{HA} \longrightarrow \mathrm{BH}^+ + \mathrm{A}^- \tag{4.2}$$

This reaction is reversible, and hence there is an equilibrium between the ionic and neutral molecular species in the PIL. In PILs, this is referred to as ionicity.

Ideally, the proton transfer of the acid to the base is complete, resulting in high inonicity. PILs are generally made by acid and base combinations that have a large ΔpK_a,

$$\Delta pK_a = pK_{a,base} - pK_{a,acid} \tag{4.3}$$

PILs with a $\Delta pK_a > 8$ has been shown to result in high ionicity, having nearly ideal Walden behaviour.[137] Mixtures made using smaller ΔpK_a, will result in the presence of both neutral and ionic species, and can be referred to as pseudo-protic ionic liquids or "poor" ionic liquids.

To obtain a pure ionic liquid, there must be no impurities, such as degradation products due to increased temperatures during the neutralization reaction or moisture from either reactants or the air, and the acid and base must be present in strictly equimolar amounts. While straightforward in principle, achieving such precise stoichiometry in practice is challenging, which is why a slight excess of either component often becomes the predominant impurity. Although typically present in small quantities, these deviations can still significantly influence the system's physicochemical properties. This is particularly evident in proton conduction. Contrary to the common assumption that proton transport in PILs can be accessed by the hydrogen-bonded networks and acidic species present in PILs,[138] purely stoichiometric PILs, especially in combination with high ΔpK_a and few proton acceptor sites, have been shown to exhibit limited proton conductivity. Instead, efficient proton transport often requires the presence of additional proton carriers, such as small excesses of acid or base, which act as proton shuttles.[139–141] Consequently, maximizing proton conductivity in these systems may not necessarily involve striving for perfectly stoichiometric ionic liquids. Rather, enhanced performance can be achieved by considering non-stoichiometric PILs, mixtures of PILs with additional acids or bases, or pseudo-ionic liquids, all of which facilitate more effective proton exchange.[142,143]

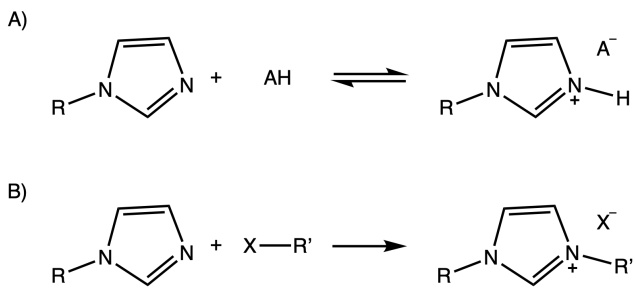

Figure 4.2: Synthesis routes to achieve A) PILs and B) AILs, showing the case of imidazole-based cations.

4.3 Aqueous imidazole

Owing to their ability to form dynamic hydrogen-bonded networks through self-association, both water and imidazole are prototypical systems for proton

transport. In the liquid state, both systems support proton transport via a combination of vehicular and proton-hopping pathways, with their relative contributions governed by factors such as temperature and pressure.[144–147] When protonated, water and imidazole exhibit closely related conduction behavior, with proton transport proceeding through analogous mechanisms and displaying similar dependencies on temperature and acid concentration.[144,146] Studies, mainly by theoretical or using diffraction and scattering techniques, have been conducted to investigate the interactions and local structure of imidazole-water systems.[148] These suggest that imidazole donates one hydrogen bond through the N^1 position and accepts hydrogen bonds at N^3, with the donating water molecules being dispersed in space and occupying sites above and below the imidazole plane.[149–151] Furthermore, imidazole has been shown to self-associate even in dilute aqueous solutions, forming dimers that adopt a variety of configurations, including hydrogen-bonded chains, T-shaped arrangements, and stacked H–π interactions.[150,152] The unprotonated N^3 position of the imidazole has been shown to facilitate strong hydrogen bonding with water molecules, with water-imidazole interaction being favorable even at higher imidazole concentrations.

Chapter 5

Methods

This thesis, with its appended papers, includes both synthesis and characterization using experimental and theoretical methods. The most work-intensive part has been the synthetic work that, while concisely summarized below, has taken a significant amount of time by including extensive and rigorous testing. Furthermore, many different experimental techniques have been necessary for characterization, all of which will be briefly introduced. Further, while the papers include some theoretical methods, which will also be briefly described, these were performed by co-authors.

5.1 Synthesis

5.1.1 Synthesis of COFs

Synthesis of COF-LZU1. Various approaches have been explored for the synthesis of COF-LZU1 in literature.[153–155] For the synthesis of the COF-LZU1 pre-network to be used further in linker-exchange experiments, four main protocols were explored. The first was that of the first reported synthesis of the net, which followed the typical protocol described in Chapter 3, using dioxane as a solvent, 3M acetic acid as the catalyst, and heating the flame-sealed vial to 120 °C for three days.[153] Small changes were implemented to this protocol, such as changing the acid amount, adding mesitylene to the mixture, as well alternative solvents, but they all yielded limited crystallinity. An alternative ambient aqueous synthesis protocol was also attempted, as it offered a less work-intensive and time-efficient method; yet, while some crystallinity could be obtained, results varied between batches and changes in the work-up protocol, hence this route was also discarded.[156] Third, the protocol developed by Deng et al.[76] for the synthesis of single crystals of TPB-DMTP-COF was translated from the structure described in their work to the structure used here (sometimes with alterations to solvent choice and modulator amounts), but yielded only very small amounts of powder that remained poorly crystalline. Finally, an alternative method was developed using microwave vials. Screening for solvent choice, modulator use, and acid amounts was performed. The resulting method

yields powders of fair crystallinity and is further described in the experimental section of **Paper III**.

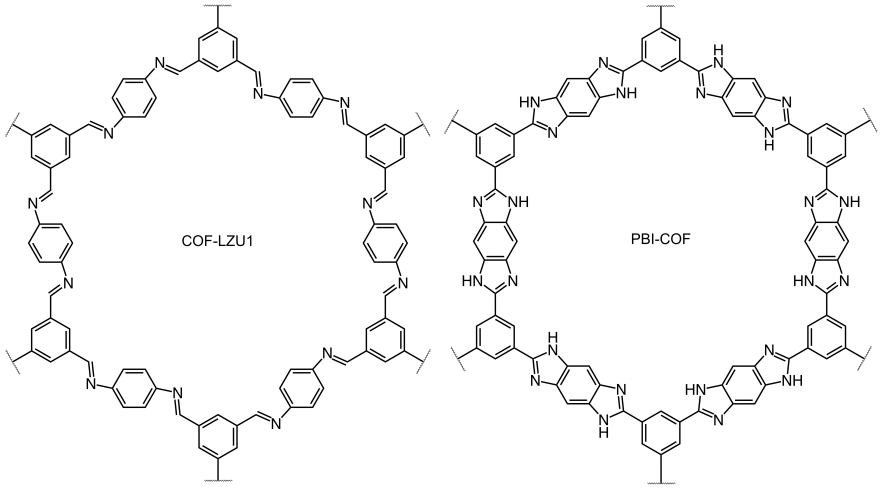

Figure 5.1: Molecular structure of COF-LZU1 and PBI-COF.

Synthesis of ILCOF-1. As for the synthesis of ILCOF-1, the first reported protocol was attempted[157] but, while yielding materials of moderate crystallinity even after further screening of conditions, the protocol developed for COF-LZU1 still resulted in higher crystallinity, as described in detail in **Paper III**.

Synthesis of imidazole-linked COFs, i.e. PBI-COF and BIP. PBI-COF[106] and BIP[105] have been reported previously as products from a cascade reaction of carbocylic acids and o-diamines, but then yield materials of lower than expected surface areas and, in the case of PBI-COF, a mostly amorphous product as interpreted by PXRD-spectra. Here, they are synthesized using a linker-exchange protocol instead. The chosen conditions are similar to those previously applied in the linker exchange procedure developed to obtain oxazoles and thiazoles,[95] but with the addition of a modulator and an alternative method for the supply of oxygen. The developed method can be used to transform the pre-networks, COF-LZU1 and ILCOF-1, to their respective analogous imidazole structures. The exact synthesis conditions can be found in the experimental section of **Paper III**.

5.1.2 Synthesis of the bases for PILs

The nitro- and cyano-functionalized bases were formed via a simple alkylation reaction. However, product purification was complicated, necessitating distillation and treatment with activated carbons. The exact procedure can be found in the experimental section of **Paper I**.

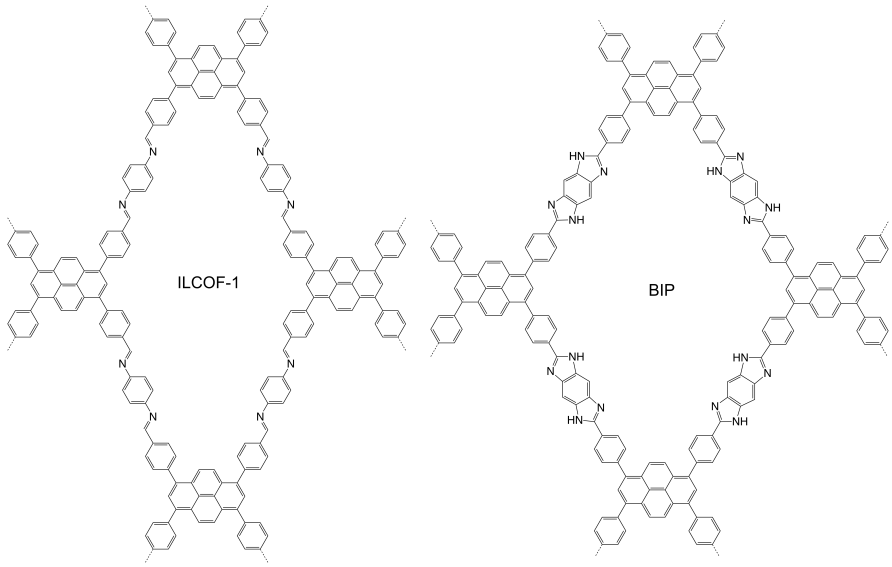

Figure 5.2: Molecular structure of ILCOF-1 and BIP.

5.1.3 Synthesis of the PILs

To synthesize as pure a protic ionic liquid as possible, avoiding water absorption, achieving as close to equimolar amounts of acid and base, reducing contamination, and avoiding thermal decomposition, a previously reported protocol was used.[158] The synthesis is done under nitrogen gas inside a fume hood, using cooling during the neutralization reaction, and takes many courses of action to ensure a good molar ratio of reagents. The exact procedure can be found in the experimental section of **Paper I**.

5.2 Characterization

5.2.1 Fourier transform infrared spectroscopy

Fourier transform infrared (FTIR) spectroscopy is an analytical technique used to identify molecular composition and structure based on the interaction of infrared (IR) radiation with a material.[159] As chemical bonds vibrate, whether they be stretching, bending, or twisting modes, if their oscillation causes a change in dipole moment and its frequency matches that of the IR radiation, the energy can be absorbed at that certain wavenumber. This resonance phenomenon between molecular vibrational modes and IR radiation is particularly useful for identifying polar bonds, which are typically strong absorbers.

In FTIR spectroscopy, a broadband infrared source emits radiation that passes through an interferometer, typically a Michelson interferometer.[159] The interferometer is made up of a beam splitter, a fixed mirror, and a moving mirror.

The incident IR beam is then divided into two, with one reflected toward the fixed mirror and the other toward the moving mirror. The recombined beams produce an interference pattern (interferogram) as a function of the optical path difference created by the moving mirror. The interferogram contains information from all IR frequencies simultaneously. After interacting with the sample, the signal is detected by an IR detector. The recorded interferogram is then transformed into a conventional spectrum (intensity versus wavenumber) using a Fourier transform (FT) algorithm.

There are different FT-IR setups available, and the best-suited choice depends on the type of sample. In this thesis, measurements were taken in either Attenuated Total Reflectance (ATR) or Diffuse Reflectance (DRIFT) mode. In ATR mode, the beam passes through an internal reflection element, on which the sample is placed.[159] This typically works well for many soft materials in the liquid or gel state. DRIFT directs the beam at the sample and collects the scattered radiation. This setup typically suits samples in powder form or samples with a rough surface.

5.2.2 Raman spectroscopy

Raman is another vibrational spectroscopy technique, but is more sensitive to polarizable bonds and is based on the inelastic scattering of monochromatic light.[160] When interacting with a laser beam, the sample scatters most of the incident light elastically, with no loss in energy. However, a very small portion of light will be scattered inelastically, due to its interaction with vibrational modes. Raman intensities at specific wavenumbers (or Raman shifts, in cm^{-1}) will hence be detected. Compared to FTIR, Raman spectroscopy is particularly sensitive to nonpolar bonds and symmetric vibrations, which may be weak or inactive in infrared spectra.

5.2.3 Nuclear magnetic resonance

Nuclear magnetic resonance (NMR) spectroscopy uses an electric field to find out information used to deduce molecular structure, dynamics, and chemical environment.[161] Atomic nuclei that possess a spin, such as ^{1}H, ^{15}N, and ^{19}F, will, when placed in a strong magnetic field, have the spin align either with or against the field. The sample is subjected to a radio-frequency pulse, and when the radiation frequency matches the resonance condition, transitions between nuclear spin states occur. When the spin relaxes, it emits radio-frequency signals that a detector measures.

Diffusion nuclear magnetic resonance (DOSY NMR) uses the same working principle as standard NMR, but applies two gradient field pulses at a delay Δ, during which the molecular species can diffuse.[162] If movement has occurred, there will be attenuation in the detected signals, which is dependent on how far the species moved during the time Δ and hence correlates to its diffusion coefficient.

5.2.4 Thermogravimetric analysis

Thermogravimetric analysis (TGA) is commonly used to study the thermal stability of samples.[163] By gradually heating a sample placed on a microbalance, any change in mass can be measured, revealing phenomena of e.g. decomposition, degradation, or vaporization. Measurements can be done at different heating rates and under different atmospheres to control the conditions and reactions that may take place. TGA curves are then commonly presented as weight percentage as a function of temperature, with changes in weight at specific temperatures revealing characteristic transitions of the material, such as the onset of decomposition and residual mass after the heat treatment.

5.2.5 Differential scanning calorimetry

Differential scanning calorimetry (DSC) is another heat-based technique, but focused on properties such as melting, crystallization, and glass transition.[164] The sample is placed into a crucible and its response to heat exchanges is compared with that of a reference (i.e. an empty pan). As the reference temperature is raised or lowered, the relative amount of heat required to keep the sample at the same temperature is measured. Where heat flow for these diverges, it will correspond to a physical or chemical transition in the sample, with endothermic processes, such as melting or evaporation, appearing as positive deviations in the DSC signal, while exothermic processes, such as crystallization or chemical reactions, release heat and appear as negative deviations. The area under the peak is proportional to the change in enthalpy associated with the transition.

5.2.6 Powder X-ray diffraction

Powder X-ray diffraction (PXRD) can be used to study crystalline materials, aiding in determining crystallographic structure, phase composition, and structural properties.[165] A monochromatic X-ray beam (here Cu$\kappa\alpha$, $\lambda = 1.5406$ Å) is directed at a sample, continuously varying the incident angle. When the X-ray interacts with the crystal lattice of the sample, it will be scattered, and the periodically arranged atoms in the crystal lattice allow for constructive interference of the reflected rays when Bragg's law is followed (Equation 5.1).

$$n\lambda = 2dsin\theta \tag{5.1}$$

where n is an integer number, λ is the wavelength of the X-ray, d is the interplanar spacing, and θ is the angle of incidence. The rays of constructive interference are measured and correlated to the angle, corresponding to a diffraction peak in the produced Intensity over 2θ spectra, indicating a crystallographic plane in the structure.

5.2.7 N_2 sorption

Nitrogen (N_2) sorption measurements are commonly performed to estimate a material's porosity, surface area, and pore size distribution.[166] These meas-

urements are based on capillary condensation and rely on the adsorption and desorption of nitrogen gas at cryogenic temperatures, generally 77 K. After activation and degassing of the sample, the sample is exposed to controlled doses of nitrogen gas, and the amount adsorbed is recorded as a function of relative pressure (P/P_0), where P is the equilibrium pressure and P_0 is the saturation vapor pressure of nitrogen at 77 K. By studying the resulting adsorption isotherm, pore volume can be estimated from the amount of nitrogen adsorbed at high relative pressures, whereby pore structure can be deduced by the isotherm shape.

5.2.8 Ionic conductivity

The setup used to measure ionic conductivity in the PILs is described in detail in a previously published work by E. M. Morais et al.[167] In short, a dip-in type conductivity microprobe was used, with samples prepared in small glass tubes inside a glovebox and the temperature was varied from 25 to 80 °C by a temperature control system.

5.2.9 Computational methods applied to COFs

Computational structure generation and screening were conducted using an in-house Python workflow tailored for layered COF systems. Node and linker building blocks were first pre-optimized using the Universal Force Field (UFF),[168] after which they were assembled into 2D COF structures using a modified version of PORMAKE.[169] The resulting single-layer geometries were subsequently pre-optimized with the machine-learned interatomic potential MACE-MH-1 with the OMOL head within the Atomic Simulation Enviroment (ASE) framework.[170–172] Based on these optimized monolayers, multilayer bulk models were constructed by systematically varying stacking arrangements. Specifically, inclined and serrated stacking modes were generated while scanning ILD and ILS, spanning configurations from AA to AB stacking. This procedure enabled the construction of an initial, coarse-grained potential energy landscape.

Electronic structure calculations were performed using CRYSTAL23 at the HSEsol-3c/sol-mSVP level of theory.[173] Relative energies were evaluated as functions of ILD and ILS to map the potential energy surface and identify low-energy candidate structures for further refinement. Selected minima were subsequently re-optimized at the same DFT level. The final structures were analyzed with respect to stacking behavior, and PXRD patterns were simulated from the optimized CIF files using the XRDCalculator module in Python Material Genomics to facilitate comparison between different stacking configurations.[174] In addition, pore characteristics, including pore size distribution, accessible surface area, and accessible pore volume, were evaluated using Zeo++.[175]

5.2.10 Computational methods applied to PILs

The search for low-energy conformers was performed using the CREST (v 2.11) software[176] with default settings, except for tight optimization and acetone implicit solvation using the GBSA model. The ten lowest-energy conformers were then used for structure refinement, which employed the r2SCAN-3c/CPCM(Ethanol) level of theory[177] in the Orca v5.0.4 software,[178] with the "TIGTHSCF" and "DEFGRID3" settings. To ensure that the lowest energy conformers were not saddle points, the lowest energy conformers for each of the three ionic liquids were submitted to numerical frequency calculations in order to determine the absence of imaginary frequencies. Only geometries with no imaginary frequencies were kept, and the rest were slightly modified and optimized again until no imaginary frequencies were present. Using the lowest single-point energy conformers of each ionic liquid, single-point calculations at the ωB97M-V/def2-TZVPD/CPCM(Ethanol)[179,180] level of theory were performed to obtain conceptual density functional theory descriptors[181] for electronegativity and electrophilicity.

Chapter 6

Results and Discussion

Having established the necessary background for the work, this chapter will discuss some of the thesis's overarching themes, summarise the results, and complement the content of the appended papers with unpublished data and learnings from the process.

Paper I investigates the effect of functionalization of the imidazolium cation of PILs with electron-withdrawing groups. As evidenced by ^{1}H NMR and FT-IR, the electron-withdrawing nitro- and cyano-groups have a deshielding effect with the resulting N-H bond being longer, and hence more acidic. This increase in acidity altered the physicochemical properties, with the PILs exhibiting increased viscosity, reduced ionic conductivity, reduced thermal stability, and increased fragility. Despite their low ionic conductivities, which preclude their use as electrolytes, this work provides new insights for the design of PILs with tunable acidity. The observed property changes also inspire further investigation of the role of fragility in this class of ILs.

Imidazole and its fundamental properties are well understood in the pure solid state, but gaps remain in our understanding of its behavior in aqueous solutions. **Paper II** delves into a spectroscopic study of aqueous imidazole. Using FI-IR, Raman, and ^{1}H NMR spectroscopy, this study complements prior knowledge, which was largely based on computational studies combined with methods that probe structural effects, such as X-ray scattering and absorption, by examining the solvation of imidazole and focusing on intermolecular interactions and mobility. Upon dilution to 0.4 mol ratio or lower, the imidazole behavior stays consistent, and as compared to pure imidazole, the peak shifts in Raman follow the same trend as those observed upon protonation of imidazole, suggesting strong $N^{3}\cdots HO$ hydrogen bond structuring. These strong imidazole-water interactions can also be inferred from IR librational modes, indicating that imidazole acts as a kosmotropic solute in water.

Paper III focuses on obtaining frameworks based on imidazole linkages using linker exchange. A synthesis method was developed that enabled access to materials with improved physicochemical properties, resulting in a substantial increase in the crystallinity of PBI-COF and a threefold increase in the surface area of BIP-COF. These materials are expected to have high thermal and

chemical stability, allow facile introduction of side chains at the NH position, and provide hydrogen donor and acceptor sites for any material used to fill the pores.

These papers all incorporate imidazole, focusing on its fundamental properties and how it can be altered, utilized, and incorporated into materials. In the following text, while some results from the appended papers will be referenced, these will not be repeated here. Rather, this chapter aims to relate them to one another and expand on them through a discussion relevant to the field and to future scientists who may continue on this line of research.

6.1 Issues encoutered during synthesis of COFs

The synthesis of COFs is extremely sensitive to the conditions used. Even though the conditions and methods may seem simple at first glance, even small differences can have detrimental effects on crystallinity. A protocol for the synthesis of the pre-network COF-LZU1 was developed for **Paper III**, yielding a crystalline structure, as evidenced by PXRD (Figures X in **Paper III**), but other commonly used protocols were first attempted. Tests using the traditional route used in the first synthesis of COF-LZU1[153] yielded diffraction spectra with a drastic decrease in intensity relative to those reported before (Figure 6.1). While this can stem from many factors, such as wet solvent or the amount of headspace in the tube after sealing, even repeated attempts yielded the same result.

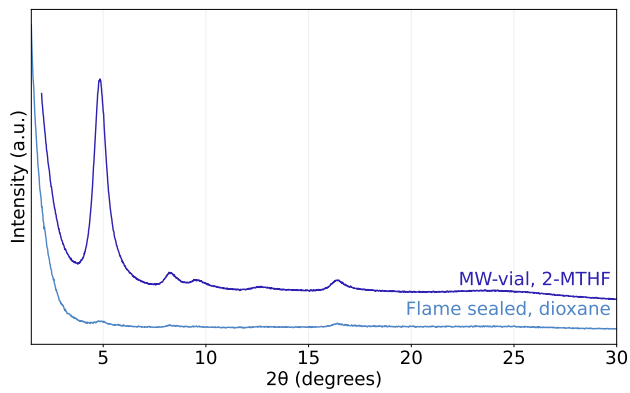

Figure 6.1: PXRD spectra of the COF-LZU1 product obtained by using the flame-sealing protocol utilizing dioxane as a solvent,[153] compared to the one obtained using the protocol in **Paper III**.

As flame-sealing remains the predominant synthesis method for COFs, and the use of dioxane as a solvent yielded limited success, alternative conditions were systematically explored. These included variations in acid strength and concentration, reagent concentrations, vial geometry, and solvent choice, however, the outcomes were generally discouraging. Representative results from this

screening of solvent and acid conditions are presented in Figure 6.2. Although minor changes in material properties were observed across these variations, no flame-sealed protocol produced materials with satisfactory crystallinity. In contrast, the ambient aqueous protocol yielded crystalline products (Figure 6.5), but reproducibility between batches was limited. This variability may be attributed to procedural factors, such as the rate of amine addition to the pre-activated aldehyde, which is only specified as "dropwise" in the reported method.

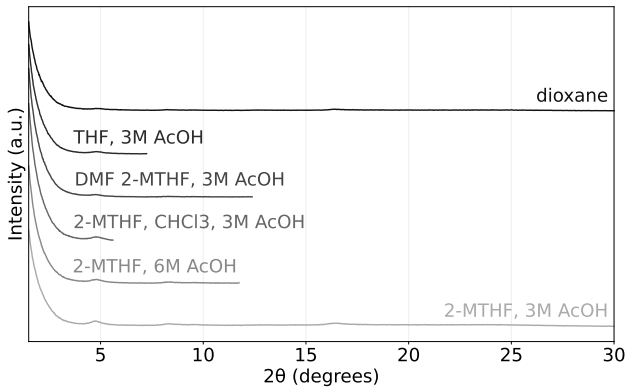

Figure 6.2: PXRD spectra of the COF-LZU1 product obtained by using the flame-sealing protocol utilizing dioxane, THF, DMF:2-MTHF(1:9), 2-MTHF:$CHCl_3$ (9:1), and 2-MTHF with either 3M or 6M acetic acid. Most scans were discontinued when the lack of crystallinity could be confirmed, having little or no peak around 5°.

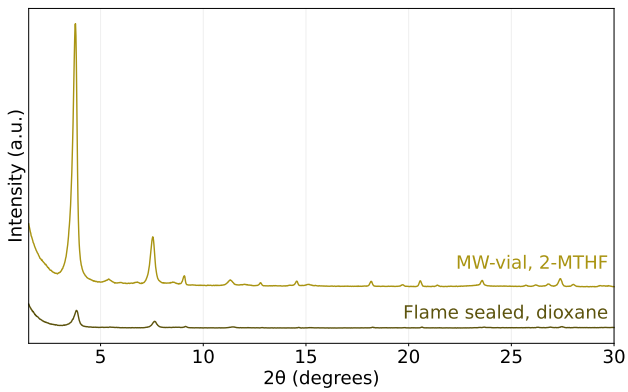

Figure 6.3: PXRD spectra of the ILCOF-1 product obtained by using the flame-sealing protocol utilizing dioxane as a solvent[157], compared to the one obtained using the synthesis conditions in **Paper III**. Both samples have been washed, though not by Soxhlet extraction, which proved necessary to remove unreacted regents, hence the small additional diffraction peaks.

Similarly to the synthesis of COF-LZU1, the previously used dioxane method yielded only limited crystallinity for ILCOF-1, whereas the microwave vial and 2-MTHF combination resulted in increased crystallinity (Figure 6.3). The estimated Brunauer–Emmett–Teller surface area using the improved protocol agrees well with values reported in other publications.[95]

6.2 The COF trilemma and the linker exchange solution

The COF trilemma, as introduced by Haase and Lotsch,[182] describes the fundamental challenge in covalent organic frameworks of balancing stability, crystallinity, and functionality, where enhancement of one property often comes at the expense of the others. **Paper III** establishes a strategy to address the trade-off between crystallinity and stability through linker exchange. This approach exploits the dynamic nature of imine chemistry to first construct a pre-organized network, which is subsequently stabilized via replacement of the linkers, effectively locking the structure in place. In this way, the resulting framework combines the structural order of the pre-network with the enhanced stability associated with imidazole linkages. Compared to a previous cascade-based synthesis of BIP, this method yields a threefold increase in surface area. Additionally, a significant improvement in crystallinity is observed for PBI-COF. Taken together, **Paper III** demonstrates that linker exchange is a viable strategy for overcoming key limitations of the COF trilemma and enabling frameworks with improved structural properties.

While the method used in **Paper III** resembles the one previously published for oxazole and thiazole linker exchange,[95] the influence of different factors on the resulting crystallinity was explored during its development. This includes parameters such as the equivalent amount of the alternative linker, different solvents and their mixtures, reaction time, the addition rate of the alternative linker, modulator use and amounts, oxidant supply, and temperature to find the optimal conditions. In contrast to the previously used method, where the oxygen needed for dehydrogenation is supplied by placing the system under oxygen, **Paper III** uses pressurized air to bubble the solution. Furthermore, a modulator was introduced, using 3 equivalents of aniline. While it might be counterintuitive to add another competitive moiety to the reaction mixture, a positive correlation between reduced reaction rate and crystallinity could be observed, both upon introduction of a modulator and upon stepwise slow addition of the alternative linker. It is also worth noting the difference in equivalence between the two structures, with PBI-COF requiring 8-12 equivalents compared to 2-4 equivalents for BIP. Respectively, these are higher and lower than the 4-8 equivalence used for the oxazole and thiazole protocols.

During the development of this method, its applicability to the formation of other heterocycles was also explored. As shown by the spectra in Figure 6.4, frameworks incorporating thiazole and oxazole linkages retained a certain degree of crystallinity, albeit to a lesser extent than their imidazole-based counterpart. In addition, a one-pot approach of the linker-exchange was investigated, which,

if successful, would have significantly reduced the synthetic effort required for imidazole-linked COFs. However, the reduced peak intensities observed in the spectra indicate that this approach adversely affected the crystallinity of the resulting materials.

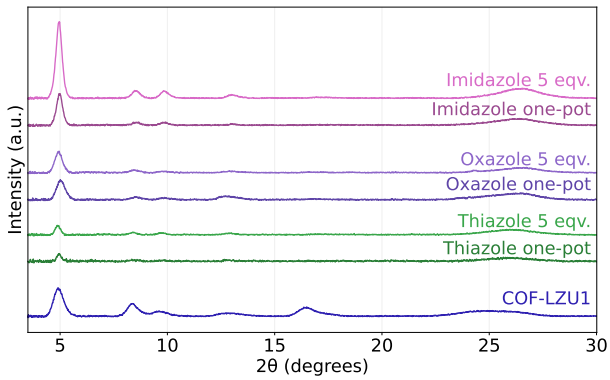

Figure 6.4: PXRD spectra of COF-LZU1 and the products formed by linker-exchange for imidazole, oxazole, and thiazole using 5 equivalents of the alternative linker and performing the synthesis either in two steps, with purification of the COF-LZU1 between, or sequentially by a one-pot method.

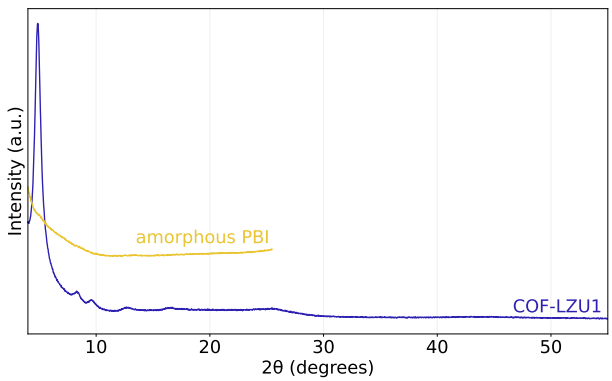

Figure 6.5: PXRD spectra of the COF-LZU1 product obtained by the ambient aqueous protocol[156] compared with the spectra obtained when utilizing the same conditions but substituting the p-phenylenediamine for 1,2,4,5-benzenetetraamine tetrachloride, yielding an amorphous product instead of PBI-COF.

The ambient aqueous protocol reported by Kong et al.,[156] initially applied to the synthesis of COF-LZU1, was also evaluated for the preparation of PBI-COF. As shown by the spectra in Figure 6.5, this method did not yield a crystalline PBI-COF. When considered alongside comparisons of material properties with previous studies (discussed in **Paper III**) that employed cascade reactions

under alternative conditions, these results further highlight the improvements achieved through the linker-exchange strategy.

6.3 Synthetic challenges encountered while alkylating nitro-functionalized imidazole

The synthesis of the nitro- and cyano-functionalized imidazole bases used in **Paper I** initially appears to be a straightforward alkylation reaction. This is indeed the case for the cyano-functionalized base, for which both ethylated and butylated derivatives were successfully synthesized on a 10–20 g scale. In contrast, the nitro-functionalized analog presented significant challenges. Although commercially available as a 97 % pure compound, tautomerization leads to the coexistence of both 4-nitroimidazole and 5-nitroimidazole isomers.[1] Consequently, alkylation results in the formation of two distinct products (Figure 6.6). Analysis of the aromatic region in the ^{1}H NMR spectra of the ethylated product obtained from small-scale reactions indicated an approximate 10:1 molar ratio of the isomers. Variations in reaction conditions, including temperature, rate of alkylating agent addition, and solvent choice, did not significantly improve selectivity. As a result, a separation method for the two species became necessary. However, due to their closely similar physicochemical properties, both chromatographic separation and distillation proved challenging. During attempted distillation, partial decomposition of the ethylated compound was observed, and the small amount of distillate obtained remained a mixture of both isomers.

These challenges ultimately informed the strategy adopted in **Paper I**, in which a butyl substituent was introduced to lower the distillation temperature. Although purification still required multiple distillation steps followed by activated carbon treatment, this approach enabled the isolation of pure 1-butyl-4-nitroimidazole.

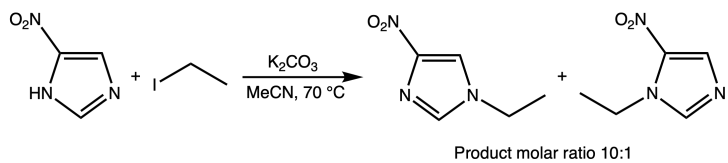

Figure 6.6: The reaction of 4(5)-nitroimidazole with iodoethane and the two products formed.

6.4 Exchangeable protons in imidazole and imidazolium

The studies in **Paper I** and **Paper II** investigate the behavior of imidazole and imidazolium with protons in greater detail. **Paper II** examines aqueous

imidazole and, using spectroscopic techniques, corroborates results reported in previous theoretical studies. When these amphoric molecules are combined, they will interact, donating and accepting hydrogen bonds from one another. This was exemplified by infrared spectroscopy, which, through shifts in the -OH peak and the emergence of a new feature in the mid-frequency region, suggested that they interact more strongly with each other than with themselves, indicating that imidazole is a kosmotropic solute. Furthermore, the merging of the -NH and -OH signals in 1D ^{1}H NMR spectra indicates that protons are in exchange between the two molecules. Moreover, aqueous imidazole, compared with pure water, was shown to affect proton dissociation from the sulfonic acid groups in a PFSA membrane, as would be expected from the increased basicity of the solution. Not showing any indication of the formation of imidazolium species, and hence no protonation of the N^3 position, the dissociated proton must be bound to water, forming excess proton complexes.

In **Paper II**, the synthesis of functionalized bases and their application as ionic liquids are investigated. The introduction of electron-withdrawing groups, such as nitro or cyano substituents, increased the acidity of the resulting ionic liquids, as evidenced by shifts in the ^{1}H NMR and IR spectra. This increase in acidity of the N-H bond, and hence the availability to dissociate the proton, was aimed at enhancing the exchange rate of the proton, as this would enable increased structural diffusion. However, the viscous character of the ionic liquid is directly correlated with proton conduction, therefore, these viscous PILs showed discouraging ionic conductivities and are not suitable as electrolytes.

The increase in acidity of the imidazolium species also means that their conjugate bases are expected to exhibit reduced basicity. Although these substituents also influence other structural and solution-phase properties, it can be hypothesized that the decreased basicity at the N^3 position diminishes its ability to facilitate proton dissociation from sulfonic acid groups in PFSA membranes. In light of this, an alternative strategy may involve incorporating proton-donating groups into the imidazole framework, thereby leveraging enhanced basicity in aqueous environments.

Chapter 7

Conclusions and Outlook

This thesis has studied imidazole in different structures and forms, including protonated imidazoum in ionic liquids and neutral imidazole in aqueous solutions, as well as imidazole as a functional linker in COFs. There has been an example of how its properties can be altered by electron-withdrawing groups, as well as how it can alter the properties of other materials, both through the dissociation behavior of protons in wetted PFSA and through its stability in COFs.

The results of these works have laid the foundation for continued studies, having gained a deeper understanding of imidazole's behavior in aqueous solution and its effect on PFSA, to better design systems that enable long-range proton mobility. Furthermore, we've developed a protocol for the synthesis of imidazole-linked COFs, which will be the natural scope of future studies once filled with water, aqueous imidazole, or acids. These solid/liquid combinations will be characterized in terms of local interactions and proton conductivity as a function of temperature.

While this thesis has explored alternative PEM materials, it has yet to implement them or combine the liquid electrolyte with a COF matrix. Having identified aqueous imidazoles effect on proton dissociation, and having gained further understanding of COFs possible role as a matrix, future work should investigate how sulfonic acid functionalities can be anchored to the COF. One way to incorporate the sulfonic acid functionalities is to include them in the linkers used, which has been previously explored,[183] although not in combination with aqueous imidazole. Another possible route is to use the COFs in **Paper III** and react the installed imidazoles with sultones, thereby introducing sulfonic acid side chains via post-functionalization.

To enable their use as PEMs, the COFs should preferably be made into a continuous, thin, and self-standing membrane. Two possible ways of achieving this that should be further explored are post-functionalization with polyether side chains and the direct synthesis of films. A recent study synthesized films with aligned pores using an especially interesting method involving kinetically trapped amorphous 3D covalent adaptable networks, which, upon evaporation of the solvent, align due to the forces induced by the drying process.[184] When

exposed to conditions that access the reversibility of the imine bonds, these amorphous films could be transformed into continuous films of 2D COFs with aligned pores. Hence, if, following the transition into 2D COFs, the films were exposed to the same linker-exchange method used in **Paper III**, they might form their imidazole-linked counterpart. Another way is the use of oligoether side chains, which have been shown to allow for the delamination of the sheets into trifluoroacetic acid water mixtures and subsequent casting into membranes.[185] Using an alkylation reaction like the one used in **Paper I**, the COF structures obtained in **Paper III** can be post-functionalized, and might then become solution processable. If such membranes are synthesized, they will be tested in operating fuel cell systems through collaborations with other researchers.

Paper II also showed that electron-withdrawing groups increased the fragility of the ionic liquid. With fragility not yet fully understood in ionic liquids, attention should be paid to exploring the relationships among acidity, intermolecular interactions, and fragility. Furthermore, electron-donating groups should contribute to the opposite effect on the acidity of the ionic liquid, and hence the conjugate acid should be stronger, which, when in an aqueous solution, might contribute to an even higher degree of dissociation of the sulfonic acid group protons.

Bibliography

(1) Tolomeu, H. V.; Fraga, C. A. M. *Molecules* **2023**, *28*, 838 (cit. on pp. 3, 48).

(2) Khabnadideh, S.; Rezaei, Z.; Khalafi-Nezhad, A.; Bahrinajafi, R.; Mohamadi, R.; Farrokhroz, A. *Bioorg. Med. Chem. Lett.* **2003**, *13*, 2863–2865 (cit. on p. 4).

(3) Moraski, G. C.; Thanassi, J. A.; Podos, S. D.; Pucci, M. J.; Miller, M. J. *J. Antibiot.* **2011**, *64*, 667–671 (cit. on p. 4).

(4) Toja, E.; Selva, D.; Schiatti, P. *J. Med. Chem.* **1984**, *27*, 610–616 (cit. on p. 4).

(5) Park, N.-H.; Shin, K.-H.; Kang, M. K. *Pharmacol. Ther. Dent.* **2017**, *10*, 488–503 (cit. on p. 4).

(6) Antonini, I.; Claudi, F.; Cristalli, G.; Franchetti, P.; Grifantini, M.; Martelli, S. *J. Med. Chem.* **1988**, *31*, 260–264 (cit. on p. 4).

(7) Office of Fossil Energy, U. S. D. o. E. Hydrogen Strategy, Enabling a Low-Carbon Economy. `https://www.energy.gov/sites/prod/files/2020/07/f76/USDOE_FE_Hydrogen_Strategy_July2020.pdf`, (accessed: 2026-03-23) (cit. on pp. 7, 8).

(8) Palo, D. R.; Dagle, R. A.; Holladay, J. D. *Chem. Rev.* **2007**, *107*, 3992–4021 (cit. on p. 7).

(9) AlHumaidan, F. S.; Halabi, M. A.; Rana, M. S.; Vinoba, M. *Energy Convers. Manage.* **2023**, *283*, 116840 (cit. on p. 8).

(10) Mokrzycki, E.; Gawlik, L. *Energies* **2024**, *17* (cit. on p. 8).

(11) Guo, R.; Li, Q.; Zhao, N. *Energy Rep.* **2022**, *8*, 884–892 (cit. on p. 8).

(12) Peighambardoust, S.; Rowshanzamir, S.; Amjadi, M. *Int. J. Hydrog. Energy* **2010**, *35*, 9349–9384 (cit. on pp. 8, 9, 11, 12).

(13) Ritchie, H. Sector by sector: where do global greenhouse gas emissions come from? `https://archive.ourworldindata.org/20251125-173858/ghg-emissions-by-sector.html` (cit. on p. 8).

(14) Liu, Y. T.; Liu, S.; Li, G. R.; Gao, X. P. *Adv. Mater.* **2021**, *33*, 2003955 (cit. on p. 8).

(15) Møller, K. T.; Jensen, T. R.; Akiba, E.; wen Li, H. *Prog. Nat. Sci. Mater. Int.* **2017**, *27*, 34–40 (cit. on p. 8).

(16) Sezer, N.; Bayhan, S.; Fesli, U.; Sanfilippo, A. *Mater. Sci. Energy Technol.* **2025**, *8*, 44–65 (cit. on p. 8).

(17) Miyatake, K. In Springer New York: 2013, pp 179–215 (cit. on pp. 9, 11, 12).

(18) Kusoglu, A.; Weber, A. Z. *Chem. Rev.* **2017**, *117*, 987–1104 (cit. on pp. 9, 11, 12).

(19) Sammes, N.; Bove, R.; Stahl, K. *Curr. Opin. Solid State and Mater. Sci.* **2004**, *8*, 372–378 (cit. on pp. 9, 13).

(20) McLean, G *Int. J. Hydrog. Energy* **2002**, *27*, 507–526 (cit. on p. 9).

(21) Breeze, P. In Elsevier: 2014, pp 129–152 (cit. on p. 9).

(22) Sharma, P.; Pandey, O. In Elsevier: 2022, pp 1–24 (cit. on pp. 9, 10).

(23) Yoshida, N.; Ishisaki, T.; Watakabe, A.; Yoshitake, M. *Electrochim. Acta* **1998**, *43*, 3749–3754 (cit. on p. 11).

(24) Arcella, V.; Troglia, C.; Ghielmi, A. *Ind. Eng. Chem. Res.* **2005**, *44*, 7646–7651 (cit. on p. 11).

(25) Deng, X.; Ma, L.; Wang, C.; Ye, H.; Cao, L.; Zhan, X.; Tian, J.; Tong, X. *Catalysts* **2025**, *15*, 74 (cit. on p. 11).

(26) Yeo, S. C.; Eisenberg, A. *J. Appl. Polym. Sci.* **1977**, *21*, 875–898 (cit. on p. 12).

(27) Osborn, S. J.; Hassan, M. K.; Divoux, G. M.; Rhoades, D. W.; Mauritz, K. A.; Moore, R. B. *Macromolecules* **2007**, *40*, 3886–3890 (cit. on p. 12).

(28) Brunn, H.; Arnold, G.; Körner, W.; Rippen, G.; Steinhäuser, K. G.; Valentin, I. *Environ. Sci. Eur.* **2023**, *35*, 20 (cit. on pp. 12, 13).

(29) Xiao, T.; Wang, R.; Chang, Z.; Fang, Z.; Zhu, Z.; Xu, C. *Prog. Nat. Sci.: Mater. Int.* **2020**, *30*, 743–750 (cit. on p. 13).

(30) Zucconi, A.; Hack, J.; Stocker, R.; Suter, T. A.; Rettie, A. J.; Brett, D. J. *J. Mater. Chem. A* **2024**, *12*, 8014–8064 (cit. on p. 13).

(31) Villers, D.; Jacques-Bedard, X.; Dodelet, J.-P. *J. Electrochem. Soc.* **2004**, *151*, A1507 (cit. on p. 13).

(32) Oh, H.-S.; Oh, J.-G.; Roh, B.; Hwang, I.; Kim, H. *Electrochem. Commun.* **2011**, *13*, 879–881 (cit. on p. 13).

(33) Li, X.; Ma, H.; Wang, H.; Zhang, S.; Jiang, Z.; Liu, B.; Guiver, M. D. *RSC Adv.* **2015**, *5*, 53870–53873 (cit. on pp. 13, 14).

(34) Araya, S. S.; Zhou, F.; Liso, V.; Sahlin, S. L.; Vang, J. R.; Thomas, S.; Gao, X.; Jeppesen, C.; Kær, S. K. *Int. J. Hydrog. Energy* **2016**, *41*, 21310–21344 (cit. on pp. 13, 14).

(35) Wang, J.-T.; Savinell, R.; Wainright, J.; Litt, M.; Yu, H. *Electrochim. Acta* **1996**, *41*, 193–197 (cit. on p. 14).

(36) Bose, S.; Kuila, T.; Nguyen, T. X. H.; Kim, N. H.; tak Lau, K.; Lee, J. H. *Prog. Polym. Sci.* **2011**, *36*, 813–843 (cit. on p. 14).

(37) Park, J.; Wang, L.; Advani, S. G.; Prasad, A. K. *Electrochim. Acta* **2014**, *120*, 30–38 (cit. on p. 14).

(38) Côté, A. P.; Benin, A. I.; Ockwig, N. W.; O'Keeffe, M.; Matzger, A. J.; Yaghi, O. M. *Science* **2005**, *310*, 1166–1170 (cit. on pp. 15, 19, 23).

(39) Uribe-Romo, F. J.; Hunt, J. R.; Furukawa, H.; Klöck, C.; O'Keeffe, M.; Yaghi, O. M. *J. Am. Chem. Soc.* **2009**, *131*, 4570–4571 (cit. on pp. 15, 23).

(40) Vardhan, H.; Nafady, A.; Al-Enizi, A. M.; Ma, S. *Nanoscale* **2019**, *11*, 21679–21708 (cit. on p. 16).

(41) Wang, Z.; Zhang, S.; Chen, Y.; Zhang, Z.; Ma, S. *Chem. Soc. Rev.* **2020**, *49*, 708–735 (cit. on p. 16).

(42) Li, Y.; Zhao, L.; Bai, Y.; Feng, F. *Food Chem.* **2025**, *469*, 142495 (cit. on p. 16).

(43) Xue, R.; Liu, Y.-S.; Huang, S.-L.; Yang, G.-Y. *ACS Sens.* **2023**, *8*, 2124–2148 (cit. on p. 16).

(44) Benedetto, G.; Stolz, R. M.; Meng, Z.; Chan, J. Y. M.; Shehayeb, E. O.; Morrell, C. T.; Fabusola, G.; Elsaesser, N.; Simon, C. M.; Mirica, K. A. *J. Am. Chem. Soc.* **2025**, *147*, 43438–43452 (cit. on p. 16).

(45) Asif, M. B.; Kim, S.; Nguyen, T. S.; Mahmood, J.; Yavuz, C. T. *J. Am. Chem. Soc.* **2024**, *146*, 3567–3584 (cit. on p. 16).

(46) Tao, S.; Jiang, D. *J. Am. Chem. Soc.* **2024**, *146*, 18151–18160 (cit. on pp. 16, 28).

(47) Wang, Y.; Zhang, W.; Yang, R.; Yang, Y.; Huang, S.; Xu, J. *ACS App. Energy Mater.* **2025**, *8*, 8811–8829 (cit. on p. 16).

(48) Li, X.; Wang, Z.; Sun, J.; Gao, J.; Zhao, Y.; Cheng, P.; Aguila, B.; Ma, S.; Chen, Y.; Zhang, Z. *Chem. Commun.* **2019**, *55*, 5423–5426 (cit. on p. 16).

(49) Guo, J.; Jiang, D. *ACS Cent. Sci.* **2020**, *6*, 869–879 (cit. on p. 16).

(50) Chakraborty, A.; Roy, M.; Alam, A.; Adhikari, D.; Pachfule, P. *Green Chem.* **2024**, *26*, 9619–9651 (cit. on p. 16).

(51) Keller, N.; Bein, T. *Chem. Soc. Rev.* **2021**, *50*, 1813–1845 (cit. on p. 16).

(52) Jiang, D.; Tan, V. G. W.; Gong, Y.; Shao, H.; Mu, X.; Luo, Z.; He, S. *Chem. Rev.* **2025**, *125*, 6203–6308 (cit. on p. 16).

(53) Yaghi, O. M. *J. Am. Chem. Soc.* **2016**, *138*, 15507–15509 (cit. on p. 16).

(54) Nguyen, H. L. *Chem. Sci.* **2021**, *12*, 8632–8647 (cit. on pp. 16, 17).

(55) Wells, A. F. *Willey* **1977** (cit. on p. 16).

(56) O'keeffe, M.; Peskov, M. A.; Ramsden, S. J.; Yaghi, O. M. *Acc. Chem. Res.* **2008**, *41*, 1782–1789 (cit. on p. 16).

(57) Geng, K.; He, T.; Liu, R.; Dalapati, S.; Tan, K. T.; Li, Z.; Tao, S.; Gong, Y.; Jiang, Q.; Jiang, D. *Chem. Rev.* **2020**, *120*, 8814–8933 (cit. on pp. 17, 19).

(58) Ge, S.; Wei, K.; Peng, W.; Huang, R.; Akinlabi, E.; Xia, H.; Shahzad, M. W.; Zhang, X.; Xu, B. B.; Jiang, J. *Chem. Soc. Rev.* **2024**, *53*, 11259–11302 (cit. on p. 17).

(59) Aslam, A. A.; Amjad, S.; Irshad, A.; Kokab, O.; Ullah, M. S.; Farid, A.; Mehmood, R. A.; Hassan, S. U.; Nazir, M. S.; Ahmed, M. *Top. Curr. Chem.* **2025**, *383*, 10 (cit. on p. 17).

(60) Xiao, J.; Chen, J.; Liu, J.; Ihara, H.; Qiu, H. *Green Energy Environ.* **2023**, *8*, 1596–1618 (cit. on p. 19).

(61) Ma, T.; Kapustin, E. A.; Yin, S. X.; Liang, L.; Zhou, Z.; Niu, J.; Li, L. H.; Wang, Y.; Su, J.; Li, J.; Wang, X.; Wang, W. D.; Wang, W.; Sun, J.; Yaghi, O. M. *Science* **2018**, *361*, 48–52 (cit. on pp. 19, 20, 26).

(62) Yi, L.; Gao, Y.; Luo, S.; Wang, T.; Deng, H. *J. Am. Chem. Soc.* **2024**, *146*, 19643–19648 (cit. on p. 19).

(63) Zhang, Y.-B.; Su, J.; Furukawa, H.; Yun, Y.; Gándara, F.; Duong, A.; Zou, X.; Yaghi, O. M. *J. Am. Chem. Soc.* **2013**, *135*, 16336–16339 (cit. on p. 19).

(64) Natraj, A.; Landman, I. R.; Pelkowski, C. E.; Burke, D. W.; Kewalramani, S.; Dichtel, W. R. *J. Am. Chem. Soc.* **2024**, *146*, 16775–16786 (cit. on pp. 20, 21).

(65) Chandra, S.; Kandambeth, S.; Biswal, B. P.; Lukose, B.; Kunjir, S. M.; Chaudhary, M.; Babarao, R.; Heine, T.; Banerjee, R. *J. Am. Chem. Soc.* **2013**, *135*, 17853–17861 (cit. on p. 20).

(66) Berlanga, I.; Ruiz-González, M. L.; González-Calbet, J. M.; Fierro, J. L. G.; Mas-Ballesté, R.; Zamora, F. *Small* **2011**, *7*, 1207–1211 (cit. on p. 20).

(67) Khayum, M. A.; Kandambeth, S.; Mitra, S.; Nair, S. B.; Das, A.; Nagane, S. S.; Mukherjee, R.; Banerjee, R. *Angew. Chem.* **2016**, *128*, 15833–15837 (cit. on p. 20).

(68) Mitra, S.; Kandambeth, S.; Biswal, B. P.; M., A. K.; Choudhury, C. K.; Mehta, M.; Kaur, G.; Banerjee, S.; Prabhune, A.; Verma, S.; Roy, S.; Kharul, U. K.; Banerjee, R. *J. Am. Chem. Soc.* **2016**, *138*, 2823–2828 (cit. on p. 20).

(69) Sahabudeen, H. et al. *Angew. Chem. Int. Ed.* **2020**, *59*, 6028–6036 (cit. on p. 20).

(70) Liu, X.-H.; Guan, C.-Z.; Ding, S.-Y.; Wang, W.; Yan, H.-J.; Wang, D.; Wan, L.-J. *J. Am. Chem. Soc.* **2013**, *135*, 10470–10474 (cit. on p. 20).

(71) Bisbey, R. P.; DeBlase, C. R.; Smith, B. J.; Dichtel, W. R. *J. Am. Chem. Soc.* **2016**, *138*, 11433–11436 (cit. on p. 20).

(72) Matsumoto, M.; Valentino, L.; Stiehl, G. M.; Balch, H. B.; Corcos, A. R.; Wang, F.; Ralph, D. C.; Mariñas, B. J.; Dichtel, W. R. *Chem* **2018**, *4*, 308–317 (cit. on p. 20).

(73) Medina, D. D.; Rotter, J. M.; Hu, Y.; Dogru, M.; Werner, V.; Auras, F.; Markiewicz, J. T.; Knochel, P.; Bein, T. *J. Am. Chem. Soc.* **2015**, *137*, 1016–1019 (cit. on p. 20).

(74) Smith, B. J.; Overholts, A. C.; Hwang, N.; Dichtel, W. R. *Chem. Commun.* **2016**, *52*, 3690–3693 (cit. on pp. 20, 25, 27).

(75) Kang, C.; Yang, K.; Zhang, Z.; Usadi, A. K.; Calabro, D. C.; Baugh, L. S.; Wang, Y.; Jiang, J.; Zou, X.; Huang, Z.; Zhao, D. *Nature Commun.* **2022**, *13*, 1370 (cit. on p. 21).

(76) Deng, L.; Chen, W.; Zhou, G.; Liu, Y.; Liu, L.; Han, Y.; Huang, Z.; Jiang, D. *J. Am. Chem. Soc.* **2024**, *146*, 35437 (cit. on pp. 21, 35).

(77) Gruber, C. G.; Frey, L.; Guntermann, R.; Medina, D. D.; Cortés, E. *Nature* **2024**, *630*, 872–877 (cit. on p. 21).

(78) Feriante, C.; Evans, A. M.; Jhulki, S.; Castano, I.; Strauss, M. J.; Barlow, S.; Dichtel, W. R.; Marder, S. R. *J. Am. Chem. Soc.* **2020**, *142*, 18637–18644 (cit. on p. 21).

(79) Khalil, S.; Sun, M.; Yang, Z.; Marciel, A. B.; Jones, M. R.; Verduzco, R. *Small* **2025**, *21* (cit. on p. 21).

(80) LaMer, V. K.; Dinegar, R. H. *J. Am. Chem. Soc.* **1950**, *72*, 4847–4854 (cit. on p. 21).

(81) Li, H.; Evans, A. M.; Castano, I.; Strauss, M. J.; Dichtel, W. R.; Bredas, J. L. *J. Am. Chem. Soc.* **2020**, *142*, 1367–1374 (cit. on p. 21).

(82) Nguyen, V.; Grünwald, M. *J. Am. Chem. Soc.* **2018**, *140*, 3306–3311 (cit. on p. 22).

(83) Hu, J.; Gupta, S. K.; Ozdemir, J.; Beyzavi, H. *ACS Appl. Nano Mater.* **2020**, *3*, 6239–6269 (cit. on p. 22).

(84) Zhu, Y.-L.; Zhao, H.-Y.; Fu, C.-L.; Li, Z.-W.; Sun, Z.-Y.; Lu, Z. *J. Phys. Chem. Lett.* **2020**, *11*, 9952–9956 (cit. on p. 22).

(85) Kuhn, P.; Antonietti, M.; Thomas, A. *Angew. Chem. Int. Ed.* **2008**, *47*, 3450–3453 (cit. on p. 23).

(86) Lyu, H.; Diercks, C. S.; Zhu, C.; Yaghi, O. M. *J. Am. Chem. Soc.* **2019**, *141*, 6848–6852 (cit. on p. 23).

(87) Wei, S.; Zhang, W.; Qiang, P.; Yu, K.; Fu, X.; Wu, D.; Bi, S.; Zhang, F. *J. Am. Chem. Soc.* **2019**, *141*, 14272–14279 (cit. on p. 23).

(88) Xu, J.; He, Y.; Bi, S.; Wang, M.; Yang, P.; Wu, D.; Wang, J.; Zhang, F. *Angew. Chem.* **2019**, *58*, 12065–12069 (cit. on p. 23).

(89) Chen, R.; Shi, J. L.; Ma, Y.; Lin, G.; Lang, X.; Wang, C. *Angew. Chem.* **2019**, *58*, 6430–6434 (cit. on p. 23).

(90) Wang, S.; Li, X. X.; Da, L.; Wang, Y.; Xiang, Z.; Wang, W.; Zhang, Y. B.; Cao, D. *J. Am. Chem. Soc.* **2021**, *143*, 15562–15566 (cit. on p. 23).

(91) Huang, N.; Lee, K. H.; Yue, Y.; Xu, X.; Irle, S.; Jiang, Q.; Jiang, D. *Angew. Chem.* **2020**, *59*, 16587–16593 (cit. on p. 23).

(92) Zhang, B.; Wei, M.; Mao, H.; Pei, X.; Alshmimri, S. A.; Reimer, J. A.; Yaghi, O. M. *J. Am. Chem. Soc.* **2018**, *140*, 12715–12719 (cit. on p. 23).

(93) Lu, M.; Zhang, M.; Liu, C. G.; Liu, J.; Shang, L. J.; Wang, M.; Chang, J. N.; Li, S. L.; Lan, Y. Q. *Angew. Chem.* **2021**, *60*, 4864–4871 (cit. on p. 23).

(94) Guan, X.; Li, H.; Ma, Y.; Xue, M.; Fang, Q.; Yan, Y.; Valtchev, V.; Qiu, S. *Nat. Chem.* **2019**, *11*, 587–594 (cit. on p. 23).

(95) Waller, P. J.; Alfaraj, Y. S.; Diercks, C. S.; Jarenwattananon, N. N.; Yaghi, O. M. *J. Am. Chem. Soc.* **2018**, *140*, 9099–9103 (cit. on pp. 23, 36, 46).

(96) Seo, J. M.; Noh, H. J.; Jeong, H. Y.; Baek, J. B. *J. Am. Chem. Soc.* **2019**, *141*, 11786–11790 (cit. on p. 23).

(97) Wang, K.; Jia, Z.; Bai, Y.; Wang, X.; Hodgkiss, S. E.; Chen, L.; Chong, S. Y.; Wang, X.; Yang, H.; Xu, Y.; Feng, F.; Ward, J. W.; Cooper, A. I. *J. Am. Chem. Soc.* **2020**, *142*, 11131–11138 (cit. on p. 23).

(98) Han, X.; Zhou, Z.; Wang, K.; Zheng, Z.; Neumann, S. E.; Zhang, H.; Ma, T.; Yaghi, O. M. *J. Am. Chem. Soc.* **2024**, *146*, 89–94 (cit. on p. 23).

(99) Kurandina, D.; Huang, B.; Xu, W.; Hanikel, N.; Darù, A.; Stroscio, G. D.; Wang, K.; Gagliardi, L.; Toste, F. D.; Yaghi, O. M. *Angew. Chem.* **2023**, *62*, e202307674 (cit. on p. 23).

(100) Kandambeth, S.; Mallick, A.; Lukose, B.; Mane, M. V.; Heine, T.; Banerjee, R. *J. Am. Chem. Soc.* **2012**, *134*, 19524–19527 (cit. on p. 23).

(101) Schiff, H. *Justus Liebigs Ann. Chem.* **1864**, *131*, 118–119 (cit. on p. 25).

(102) Patil, R. D.; Adimurthy, S. *Asian J. Org. Chem.* **2013**, *2*, 726–744 (cit. on p. 25).

(103) Wang, P. L.; Ding, S. Y.; Zhang, Z. C.; Wang, Z. P.; Wang, W. *J. Am. Chem. Soc.* **2019**, *141*, 18004–18008 (cit. on pp. 25, 26).

(104) Zhang, Y.; Qiao, Z.; Zhang, R.; Wang, Z.; Wang, H. J.; Zhao, J.; Cao, D.; Wang, S. *Angew. Chem.* **2023**, *62*, e202314539 (cit. on p. 25).

(105) Ranjeesh, K. C.; Illathvalappil, R.; Veer, S. D.; Peter, J.; Wakchaure, V. C.; Goudappagouda; Raj, K. V.; Kurungot, S.; Babu, S. S. *J. Am. Chem. Soc.* **2019**, *141*, 14950–14954 (cit. on pp. 25, 26, 28, 36).

(106) Zhang, J.; Kong, Y.-R.; Liu, Y.; Luo, H.-B.; Zou, Y.; Zang, S.-Q.; Ren, X.-M. *ACS Mater. Lett.* **2022**, *4*, 2597–2603 (cit. on pp. 25, 28, 36).

(107) Hermes, S.; Witte, T.; Hikov, T.; Zacher, D.; Bahnmüller, S.; Langstein, G.; Huber, K.; Fischer, R. A. *J. Am. Chem. Soc.* **2007**, *129*, 5324–5325 (cit. on p. 26).

(108) Tsuruoka, T.; Furukawa, S.; Takashima, Y.; Yoshida, K.; Isoda, S.; Kitagawa, S. *Angew. Chem. Int. Ed.* **2009**, *48*, 4739–4743 (cit. on p. 26).

(109) Schaate, A.; Roy, P.; Godt, A.; Lippke, J.; Waltz, F.; Wiebcke, M.; Behrens, P. *Chem. – A Eur. J.* **2011**, *17*, 6643–6651 (cit. on p. 26).

(110) Smith, B. J.; Dichtel, W. R. *J. Am. Chem. Soc.* **2014**, *136*, 8783–8789 (cit. on p. 26).

(111) Calik, M.; Sick, T.; Dogru, M.; Döblinger, M.; Datz, S.; Budde, H.; Hartschuh, A.; Auras, F.; Bein, T. *J. Am. Chem. Soc.* **2016**, *138*, 1234–1239 (cit. on p. 26).

(112) Zhang, J.; Wang, Z.; Suo, J.; Tuo, C.; Chen, F.; Chang, J.; Zheng, H.; Li, H.; Zhang, D.; Fang, Q.; Qiu, S. *J. Am. Chem. Soc.* **2024**, *146*, 35090–35097 (cit. on p. 27).

(113) Wang, S.; Zhang, Z.; Zhang, H.; Rajan, A. G.; Xu, N.; Yang, Y.; Zeng, Y.; Liu, P.; Zhang, X.; Mao, Q.; He, Y.; Zhao, J.; Li, B.-G.; Strano, M. S.; Wang, W.-J. *Matter* **2019**, *1*, 1592–1605 (cit. on p. 27).

(114) Tohidi, M. E.; Amiri, A. *Adv. Mater.* **2026**, *38* (cit. on p. 27).

(115) Li, Z.; Ding, X.; Feng, Y.; Feng, W.; Han, B. H. *Macromolecules* **2019**, *52*, 1257–1265 (cit. on p. 27).

(116) Qian, C.; Qi, Q. Y.; Jiang, G. F.; Cui, F. Z.; Tian, Y.; Zhao, X. *J. Am. Chem. Soc.* **2017**, *139*, 6736–6743 (cit. on p. 27).

(117) Qian, H. L.; Li, Y.; Yan, X. P. *J. of Mater. Chem. A* **2018**, *6*, 17307–17311 (cit. on p. 27).

(118) Zhai, Y.; Liu, G.; Jin, F.; Zhang, Y.; Gong, X.; Miao, Z.; Li, J.; Zhang, M.; Cui, Y.; Zhang, L.; Liu, Y.; Zhang, H.; Zhao, Y.; Zeng, Y. *Angew. Chem. Int. Ed.* **2019**, *58*, 17679–17683 (cit. on p. 27).

(119) Waller, P. J.; Alfaraj, Y. S.; Diercks, C. S.; Jarenwattananon, N. N.; Yaghi, O. M. *J. Am. Chem. Soc* **2018**, *140*, 9099–9103 (cit. on p. 27).

(120) Lu, Y.; Zhou, S.; Zhu, C.; Zhou, J.; Feng, X. *Chem. Eur. J.* **2025**, *31* (cit. on p. 28).

(121) Chandra, S.; Kundu, T.; Dey, K.; Addicoat, M.; Heine, T.; Banerjee, R. *Chem. Mater.* **2016**, *28*, 1489–1494 (cit. on p. 28).

(122) Yang, Y.; He, X.; Zhang, P.; Andaloussi, Y. H.; Zhang, H.; Jiang, Z.; Chen, Y.; Ma, S.; Cheng, P.; Zhang, Z. *Angew. Chem.* **2020**, *132*, 3707–3713 (cit. on p. 28).

(123) Tao, S.; Zhai, L.; Wonanke, A. D. D.; Addicoat, M. A.; Jiang, Q.; Jiang, D. *Nature Commun.* **2020**, *11*, 1981 (cit. on p. 28).

(124) Luan, T.-X.; Wang, Q.; Zhang, P.; Li, W.; Kong, S.; Feng, Y.; Yuan, S.; Li, P.-Z. *Sci. China Mater.* **2024**, *67*, 125–133 (cit. on p. 28).

(125) Fu, Y.; Wu, Y.; Chen, S.; Zhang, W.; Zhang, Y.; Yan, T.; Yang, B.; Ma, H. *ACS Nano* **2021**, *15*, 19743–19755 (cit. on p. 29).

(126) Hao, L.; Jia, S.; Qiao, X.; Lin, E.; Yang, Y.; Chen, Y.; Cheng, P.; Zhang, Z. *Angew. Chem.* **2023**, *135* (cit. on p. 29).

(127) Guo, Y.; Zou, X.; Li, W.; Hu, Y.; Jin, Z.; Sun, Z.; Gong, S.; Guo, S.; Yan, F. *J. Mater. Chem. A* **2022**, *10*, 6499–6507 (cit. on p. 29).

(128) Wang, Z.; Zheng, W.; Li, B.; Sun, W.; Zhao, L.; Yuan, W. *Chem. Eng. J.* **2022**, *433*, 133749 (cit. on p. 29).

(129) Cao, L.; Wu, H.; Cao, Y.; Fan, C.; Zhao, R.; He, X.; Yang, P.; Shi, B.; You, X.; Jiang, Z. *Adv. Mater.* **2020**, *32* (cit. on p. 29).

(130) Popov, I.; Zhu, Z.; Singh, H.; Abdullah, M.; Sacci, R. L.; Mamontov, E.; Damron, J. T.; Gainaru, C.; Paddison, S. J.; Sokolov, A. P. *Cell Rep. Phys. Sci.* **2024**, *5*, 102294 (cit. on p. 31).

(131) Kreuer, K.; Rabenau, A.; Weppner, W. *Angew. Chem. Int. Ed.* **1982**, *21*, 208–209 (cit. on p. 31).

(132) Agmon, N. *Chem. Phys. Lett.* **1995**, *244*, 456–462 (cit. on p. 31).

(133) Popov, I.; Zhu, Z.; Young-Gonzales, A. R.; Sacci, R. L.; Mamontov, E.; Gainaru, C.; Paddison, S. J.; Sokolov, A. P. *Commun. Chem.* **2023**, *6*, 77 (cit. on p. 31).

(134) Doi, H.; Song, X.; Minofar, B.; Kanzaki, R.; Takamuku, T.; Umebayashi, Y. *Chem. Eur. J.* **2013**, *19*, 11522–11526 (cit. on p. 31).

(135) Anouti, M.; Jacquemin, J.; Porion, P. *J. Phys. Chem. B* **2012**, *116*, 4228–4238 (cit. on p. 31).

(136) Greaves, T. L.; Drummond, C. J. *Chem. Rev.* **2008**, *108*, 206–237 (cit. on p. 32).

(137) Belieres, J.-P.; Angell, C. A. *J. Phys. Chem. B* **2007**, *111*, 4926–4937 (cit. on p. 33).

(138) Wong, C. Y.; Wong, W. Y.; Loh, K. S.; Lim, K. L. *React. Funct. Polym.* **2022**, *171*, 105160 (cit. on p. 33).

(139) Smith, D. E.; Walsh, D. A. *Adv. Energy Mater.* **2019**, *9* (cit. on p. 33).

(140) Yaghini, N.; Gómez-González, V.; Varela, L. M.; Martinelli, A. *Phys. Chem. Chem, Phys.* **2016**, *18*, 23195–23206 (cit. on p. 33).

(141) Hoarfrost, M. L.; Tyagi, M.; Segalman, R. A.; Reimer, J. A. *J. Phys. Chem. B* **2012**, *116*, 8201–8209 (cit. on p. 33).

(142) Watanabe, H.; Arai, N.; Jihae, H.; Kawana, Y.; Umebayashi, Y. *J. Mol. Liq.* **2022**, *352*, 118705 (cit. on p. 33).

(143) Hasani, M.; Varela, L. M.; Martinelli, A. *J. Phys. Chem. B* **2020** (cit. on p. 33).

(144) Kreuer, K.-D. *Chem. Mater.* **1996**, *8*, 610–641 (cit. on p. 34).

(145) Kreuer, K. *Solid State Ion.* **1997**, *94*, 55–62 (cit. on p. 34).

(146) Kreuer, K.-D.; Fuchs, A.; Ise, M.; Spaeth, M.; Maier, J. *Electrochim. Acta* **1998**, *43*, 1281–1288 (cit. on p. 34).

(147) Munch, W.; Kreuer, K.-D.; Silvestri, W.; Maier, J.; Seifert, G. *Solid State Ion.* **2001**, *145*, 437–443 (cit. on p. 34).

(148) Malloum, A.; Conradie, J. *J. Mol. Model.* **2025**, *31*, 278 (cit. on p. 34).

(149) Duboué-Dijon, E.; Mason, P. E.; Fischer, H. E.; Jungwirth, P. *J. Chem. Phys.* **2017**, *146* (cit. on p. 34).

(150) Pagliai, M.; Funghi, G.; Vassetti, D.; Procacci, P.; Chelli, R.; Cardini, G. *J. Phys. Chem. B* **2019**, *123*, 4055–4064 (cit. on p. 34).

(151) Al-Madhagi, L. H.; Callear, S. K.; Schroeder, S. L. *Phys. Chem. Chem. Phys.* **2020**, *22*, 5105–5113 (cit. on p. 34).

(152) Liem, S. Y.; Shaik, M. S.; Popelier, P. L. A. *J. Phys. Chem. B* **2011**, *115*, 11389–11398 (cit. on p. 34).

(153) Ding, S. Y.; Gao, J.; Wang, Q.; Zhang, Y.; Song, W. G.; Su, C. Y.; Wang, W. (cit. on pp. 35, 44).

(154) Xiao, Y.; Ling, Y.; Wang, K.; Ren, S.; Ma, Y.; Li, L. *J. Am. Chem. Soc.* **2023**, *145*, 13537–13541 (cit. on p. 35).

(155) Kong, X.; Wu, Z.; Strømme, M.; Xu, C. *J. Am. Chem. Soc.* **2024**, *146*, 742–751 (cit. on p. 35).

(156) Kong, X.; Wu, Z.; Strømme, M.; Xu, C. *J. Am. Chem. Soc.* **2024**, *146*, 742–751 (cit. on pp. 35, 47).

(157) Rabbani, M. G.; Sekizkardes, A. K.; Kahveci, Z.; Reich, T. E.; Ding, R.; El-Kaderi, H. M. *Chem. Eur. J.* **2013**, *19*, 3324–3328 (cit. on pp. 36, 45).

(158) Morais, E. M.; Abdurrokhman, I.; Martinelli, A. *J. Mol. Liq.* **2022**, *360*, 119358 (cit. on p. 37).

(159) Khan, S. A.; Khan, S. B.; Khan, L. U.; Farooq, A.; Akhtar, K.; Asiri, A. M. In Springer International Publishing: 2018, pp 317–344 (cit. on pp. 37, 38).

(160) Moore, D. In Wiley: 2014, pp 1813–1830 (cit. on p. 38).

(161) Jacobsen, N. E., *NMR Spectroscopy Explained*; Wiley: 2007 (cit. on p. 38).

(162) Claridge, T. D. In Elsevier: 2009, pp 303–334 (cit. on p. 38).

(163) Vyazovkin, S. In Wiley: 2012, pp 1–12 (cit. on p. 39).

(164) Schick, C.; Lexa, D.; Leibowitz, L. In Wiley: 2012, pp 1–13 (cit. on p. 39).

(165) Holder, C. F.; Schaak, R. E. *Nano* **2019**, *13*, 7359–7365 (cit. on p. 39).

(166) Liu, P.; Chen, G. In Elsevier: 2014, pp 411–492 (cit. on p. 39).

(167) Morais, E. M.; Idström, A.; Evenäs, L.; Martinelli, A. *Molecules* **2023**, *28*, 5147 (cit. on p. 40).

(168) Rappe, A. K.; Casewit, C. J.; Colwell, K. S.; Goddard, W. A. I.; Skiff, W. M. *J. Am. Chem. Soc.* **1992**, *114*, 10024–10035 (cit. on p. 40).

(169) Lee, S.; Kim, B.; Cho, H.; Lee, H.; Lee, S. Y.; Cho, E. S.; Kim, J. *Appl. Mater. Interfaces.* **2021**, *13*, 23647–23654 (cit. on p. 40).

(170) Batatia, I.; Kovacs, D. P.; Simm, G.; Ortner, C.; Csányi, G. *Adv. Neural Inf. Process. Syst.* **2022**, *35*, 11423–11436 (cit. on p. 40).

(171) Batatia, I.; Lin, C.; Hart, J.; Kasoar, E.; Elena, A. M.; Norwood, S. W.; Wolf, T.; Csányi, G. *arXiv preprint arXiv:2510.25380* **2025** (cit. on p. 40).

(172) Hjorth Larsen, A. et al. *J. Phys. Condens. Matter* **2017**, *29*, 273002 (cit. on p. 40).

(173) Erba, A.; Desmarais, J. K.; Casassa, S.; Civalleri, B.; Donà, L.; Bush, I. J.; Searle, B.; Maschio, L.; Edith-Daga, L.; Cossard, A.; Ribaldone, C.; Ascrizzi, E.; Marana, N. L.; Flament, J.-P.; Kirtman, B. *J. Chem. Theory Comput.* **2023**, *19*, 6891–6932 (cit. on p. 40).

(174) Ong, S. P.; Richards, W. D.; Jain, A.; Hautier, G.; Kocher, M.; Cholia, S.; Gunter, D.; Chevrier, V. L.; Persson, K. A.; Ceder, G. *Comput. Mater. Sci.* **2013**, *68*, 314–319 (cit. on p. 40).

(175) Willems, T. F.; Rycroft, C. H.; Kazi, M.; Meza, J. C.; Haranczyk, M. *Micropor. Mesopor. Mater.* **2012**, *149*, 134–141 (cit. on p. 40).

(176) Pracht, P.; Bohle, F.; Grimme, S. *Phys. Chem. Chem, Phys.* **2020**, *22*, 7169–7192 (cit. on p. 41).

(177) Grimme, S.; Hansen, A.; Ehlert, S.; Mewes, J.-M. *J. Chem. Phys.* **2021**, *154* (cit. on p. 41).

(178) Neese, F.; Wennmohs, F.; Becker, U.; Riplinger, C. *J. Chem. Phys.* **2020**, *152* (cit. on p. 41).

(179) Mardirossian, N.; Head-Gordon, M. *J. Chem. Phys.* **2016**, *144* (cit. on p. 41).

(180) Rappoport, D.; Furche, F. *J. Chem. Phys.* **2010**, *133* (cit. on p. 41).

(181) Geerlings, P.; De Proft, F.; Langenaeker, W. *Chem. rev.* **2003**, *103*, 1793–1874 (cit. on p. 41).

(182) Haase, F.; Lotsch, B. V. *Chem. Soc. Rev.* **2020**, *49*, 8469 (cit. on p. 46).

(183) Wang, K.; Ahn, D. D.; Rampal, N.; Thomassian, J.; Sabeva, N. S.; Kannan, O.; Borgs, C.; Chayes, J. T.; Yaghi, O. M. *J. Am. Chem. Soc.* **2026**, *148*, 10094–10104 (cit. on p. 51).

(184) Cusin, L.; Cieciórski, P.; Gele, S. V.; Heck, F.; Krause, S.; Majewski, P. W.; Lotsch, B. V.; Danowski, W.; Samorì, P. *Nat. Synth.* **2025**, *4*, 632–641 (cit. on p. 51).

(185) Senarathna, M. C.; Li, H.; Perera, S. D.; Torres-Correas, J.; Diwakara, S. D.; Boardman, S. R.; Al-Kharji, N. M.; Liu, Y.; Smaldone, R. A. *Angew. Chem. Int. Ed.* **2023**, *62* (cit. on p. 52).